



## Invited review

## Seasonal temperature and precipitation recorded in the intra-annual oxygen isotope pattern of meteoric water and tree-ring cellulose

Brian A. Schubert <sup>a,\*</sup>, A. Hope Jahren <sup>b</sup><sup>a</sup> School of Geosciences, University of Louisiana at Lafayette, 611 McKinley St, Box 43705, Lafayette, LA, 70504, USA<sup>b</sup> Department of Geology and Geophysics, University of Hawaii at Mānoa, 1680 East-West Road, POST 701, Honolulu, HI, 96822, USA

## ARTICLE INFO

## Article history:

Received 13 May 2015

Received in revised form

9 July 2015

Accepted 25 July 2015

Available online xxx

## Keywords:

Oxygen isotopes

Paleoclimate

Cellulose

Tree rings

Seasonality

Fossil wood

Meteoric water

## ABSTRACT

Modern and ancient wood is a valuable terrestrial record of carbon ultimately derived from the atmosphere and oxygen inherited from local meteoric water. Many modern and fossil wood specimens display rings sufficiently thick for intra-annual sampling, and analytical techniques are rapidly improving to allow for precise carbon and oxygen isotope measurements on very small samples, yielding unprecedented resolution of seasonal isotope records. However, the interpretation of these records across diverse environments has been problematic because a unifying model for the quantitative interpretation of seasonal climate parameters from oxygen isotopes in wood is lacking. Towards such a model, we compiled a dataset of intra-ring oxygen isotope measurements on modern wood cellulose ( $\delta^{18}\text{O}_{\text{cell}}$ ) from 33 globally distributed sites. Five of these sites represent original data produced for this study, while the data for the other 28 sites were taken from the literature. We defined the intra-annual change in oxygen isotope value of wood cellulose [ $\Delta(\delta^{18}\text{O}_{\text{cell}})$ ] as the difference between the maximum and minimum  $\delta^{18}\text{O}_{\text{cell}}$  values determined within the ring. Then, using the monthly-resolved dataset of the oxygen isotope composition of meteoric water ( $\delta^{18}\text{O}_{\text{MW}}$ ) provided by the Global Network of Isotopes in Precipitation database, we quantified the empirical relationship between the intra-annual change in meteoric water [ $\Delta(\delta^{18}\text{O}_{\text{MW}})$ ] and  $\Delta(\delta^{18}\text{O}_{\text{cell}})$ . We then used monthly-resolved datasets of temperature and precipitation to develop a global relationship between  $\Delta(\delta^{18}\text{O}_{\text{MW}})$  and maximum/minimum monthly temperatures and winter/summer precipitation amounts. By combining these relationships we produced a single equation that explains much of the variability in the intra-ring  $\delta^{18}\text{O}_{\text{cell}}$  signal through only changes in seasonal temperature and precipitation amount ( $R^2 = 0.82$ ). We show how our recent model that quantifies seasonal precipitation from intra-ring carbon isotope profiles can be incorporated into the oxygen model above in order to separately quantify both seasonal temperature and seasonal precipitation. Determination of seasonal climate variation using high-resolution isotopes in tree-ring records makes possible a new understanding of the seasonal fluctuations that control the environmental conditions to which organisms are subject, both during recent history and in the geologic past.

© 2015 Elsevier Ltd. All rights reserved.

## 1. Introduction

Multiple empirical studies have shown the oxygen isotopic composition of meteoric water ( $\delta^{18}\text{O}_{\text{MW}}$ ) to be highly correlated with various climate parameters on local, regional, and global scales (e.g., Araguás-Araguás et al., 1998; Bowen, 2008; Dansgaard, 1964; Lachniet and Patterson, 2006, 2009; Rozanski et al., 1992, 1993). One fate for meteoric water is uptake by plant roots and incorporation into plant tissues; in fact, meteoric water exerts

fundamental control on the oxygen isotope signature of plant tissues (Deniro and Epstein, 1979). Because trees are long-lived and tree fossils are abundant in the fossil record, workers have long sought to gain physiological (Gessler et al., 2009; Offermann et al., 2011) or environmental information from the oxygen isotope composition of both modern (Brienen et al., 2012; Knorre et al., 2010; Loader et al., 2010, 2007; McCarroll and Loader, 2004; Poussart et al., 2004; Rinne et al., 2013; Saurer et al., 2008; Treydte et al., 2006; Young et al., 2015) and ancient wood (Jahren and Sternberg, 2002, 2003, 2008; Richter et al., 2008a; Wolfe et al., 2012). Cellulose has been the substrate of choice because it is resistant to degradation (e.g., Griffith et al., 2008; Jahren and

\* Corresponding author.

E-mail address: schubert@louisiana.edu (B.A. Schubert).

Sternberg, 2002) and can be extracted from heterogeneous lignin complexes (Green, 1963). Multiple studies have attempted to calculate the  $\delta^{18}\text{O}_{\text{MW}}$  value from the  $\delta^{18}\text{O}$  value of wood cellulose ( $\delta^{18}\text{O}_{\text{cell}}$ ) using fractionations based on empirical datasets and experimental observations (Csank et al., 2013; Richter et al., 2008b; Saurer et al., 1997; Sternberg et al., 2007; Waterhouse et al., 2002; Yakir and DeNiro, 1990). Most of this work has been performed using whole leaf tissues or whole tree-rings due to the large amount of plant tissue required for classical isotope analysis (e.g., Sternberg, 1989). Recent advances in cellulose extraction techniques and mass spectrometry automation have allowed researchers to create high-resolution intra-ring profiles of  $\delta^{18}\text{O}_{\text{cell}}$  based upon analyses of as little as 100 µg of cellulose (e.g., Dodd et al., 2008; Schollaen et al., 2014). However, a unifying relationship for interpreting observed patterns in  $\delta^{18}\text{O}_{\text{cell}}$  extracted from across tree-rings is lacking. Multiple studies have shown that individual trees may have different  $\delta^{18}\text{O}_{\text{cell}}$  absolute values, even when growing at the same site, under the same conditions (Reynolds-Henne et al., 2009; Richter et al., 2008b; Wang et al., 1998) and authors have concluded that the search for a single environmental signal to explain absolute  $\delta^{18}\text{O}_{\text{cell}}$  values across all sites is futile (McCarroll and Loader, 2004). We have shown elsewhere that the relative change in the carbon isotope ( $\delta^{13}\text{C}$ ) values measured from intra-ring profiles provides valuable quantitative paleoclimate information, despite the fact that absolute values of  $\delta^{13}\text{C}$  in wood differed between individual trees at the same site (Schubert and Jahren, 2011). Here we sought to evaluate a similar approach for high-resolution intra-ring  $\delta^{18}\text{O}_{\text{cell}}$  measurements.

Towards this, we present new intra-ring  $\delta^{18}\text{O}_{\text{cell}}$  profiles from five widely distributed sites, and combine these new data with 28 other similar records from the literature to form a global dataset of intra-annual profiles of  $\delta^{18}\text{O}_{\text{cell}}$  from 792 tree rings measured at 33 sites. We analyze the dataset to quantify a relationship between intra-annual changes in  $\delta^{18}\text{O}_{\text{cell}}$  measured across tree rings and the intra-annual change in  $\delta^{18}\text{O}_{\text{MW}}$  across all sites. We then use these data and a global dataset of monthly  $\delta^{18}\text{O}_{\text{MW}}$  and climate data to produce an empirical relationship explaining the intra-annual  $\delta^{18}\text{O}_{\text{cell}}$  patterns observed in tree rings worldwide. Last, we combine this result with our previous work that analyzed a global intra-ring carbon isotope dataset (Schubert and Jahren, 2011) in order to produce a set of equations for quantifying seasonal climate from recent and fossil, high-resolution, tree-ring records.

## 2. Materials and methods

### 2.1. Stable isotope analysis

We sampled four consecutive rings from each of five living trees for high-resolution intra-ring  $\delta^{18}\text{O}_{\text{cell}}$  measurements. Given the consistency in the intra-annual  $\delta^{18}\text{O}_{\text{cell}}$  pattern among closely spaced trees (e.g., Zhu et al., 2012), only a single tree was sampled at each site. However, four rings per sample were analyzed in order to attain an average intra-annual signal, as the  $\delta^{18}\text{O}_{\text{cell}}$  pattern in individual tree rings within a tree can be variable from year-to-year (e.g., Schollaen et al., 2013). The trees grow at five sites within Hawaii, Japan, Alaska, and Norway (two sites), which together span more than fifty degrees of latitude, represent tropical to arctic ecosystems, and reflect a wide range of seasonal temperatures and precipitation amounts (Fig. 1). Five different genera are represented: three are evergreen (Site 1: *Sophora*; Site 4: *Picea*; and Site 5: *Tsuga*) and two are deciduous (Site 2: *Larix* and Site 3: *Metasequoia*) (Table 1). Using a razor blade, each tree ring was subsampled by hand into an average of ~14 subsamples/ring (minimum: Site 1, *Sophora*, 11 subsamples/ring; maximum: Site 5, *Tsuga*, 18 measurements/ring) to achieve the highest resolution

possible while obtaining sufficient material for cellulose extraction and stable isotope analyses. Cellulose was extracted from a total of 283 individual slices weighing between 1 and 3 mg using methods modified from Brendel et al. (2000), Gaudinski et al. (2005), and Evans and Schrag (2004). In brief, 80% acetic acid and 67.9% nitric acid were added in a 10:1 ratio, vortexed, and heated at 120 °C for 30 min. Samples were then washed twice with 99% ethanol and once with deionized water; 17% (w/v) NaOH was then added and the samples sat for 10 min. The NaOH was decanted and the samples were rinsed with a series of washes that included deionized water, acetic acid, ethanol, and acetone. The samples were then allowed to dry overnight at 50 °C. 0.45–0.55 mg of the resulting pure  $\alpha$ -cellulose samples were weighed into silver capsules and analyzed for  $\delta^{18}\text{O}_{\text{cell}}$ . The  $\delta^{18}\text{O}_{\text{cell}}$  measurements were made using a Delta V Advantage Isotope Ratio Mass Spectrometry (IRMS) instrument coupled to a High-Temperature Conversion Elemental Analyzer (Thermo Fisher, Bremen, Germany) configured with a zero-blank autosampler (Costech Analytical, Valencia, CA, USA). All  $\delta^{18}\text{O}_{\text{cell}}$  values were normalized to the VSMOW-SLAP scale using two internal laboratory  $\alpha$ -cellulose reference materials, calibrated using benzoic acid reference materials IAEA-601 (23.14‰) and IAEA-602 (71.28‰) (Brand et al., 2009). Three to six replicates of an  $\alpha$ -cellulose quality assurance sample were analyzed as unknowns in each batch run. The standard deviation of all  $\delta^{18}\text{O}_{\text{cell}}$  quality assurance samples was 0.15‰ ( $n = 64$ ) with an average value within 0.02‰ of the calibrated value.

For two of the trees (*Picea* from Palmer, Alaska, USA, Site 4; *Tsuga* from Ås, Norway, Site 5), we also produced a high-resolution, intra-ring  $\delta^{13}\text{C}$  record from the extracted cellulose. The samples were analyzed for  $\delta^{13}\text{C}$  values using the Delta V Advantage IRMS instrument coupled to a Costech ECS 4010 Elemental Analyzer (Costech Analytical, Valencia, CA, USA) with the zero-blank autosampler. The analytical uncertainty associated with each measurement was <0.1‰.

### 2.2. Published tree-ring records

We augmented our dataset with a thorough survey of previously published data, including high-resolution intra-ring  $\delta^{18}\text{O}_{\text{cell}}$  data from 19 studies from 28 sites (Fig. 1). The comprehensive dataset included high-resolution  $\delta^{18}\text{O}_{\text{cell}}$  data from a total of 792 distinct rings from 33 sites spanning 112° of latitude (Table 1). We excluded studies that only sampled earlywood and latewood (i.e., 2 measurements per ring) (e.g., Sohn et al., 2013) and studies that were limited to high-resolution measurements across only one tree ring (e.g., Li et al., 2011). The resultant dataset was taxonomically diverse and included 13 angiosperm genera (*Carapa*, *Cordia*, *Fagus*, *Gouania*, *Hieronima*, *Ocotea*, *Populus*, *Quercus*, *Rizophora*, *Samanea*, *Sophora*, *Tachigali*, and *Tectona*) and 7 conifer genera (*Larix*, *Metasequoia*, *Picea*, *Pinus*, *Podocarpus*, *Sequoia*, and *Tsuga*) (Table 1).

### 2.3. International Atomic Energy Agency (IAEA) Global Network of Isotopes in Precipitation (GNIP) database

All long-term average monthly temperature (°C), precipitation (mm), and  $\delta^{18}\text{O}_{\text{MW}}$  data were compiled from the IAEA GNIP database, unless noted. Because the database is regularly updated as new data are submitted and verified, the station names and data used for our analysis are provided in Supplementary Table 3. Taken in total, these sites span 158° of latitude ranging from 82.5 °N (Alert, Nunavut, Canada) to 75.6 °S (Halley Bay, Antarctica) (Fig. 1).

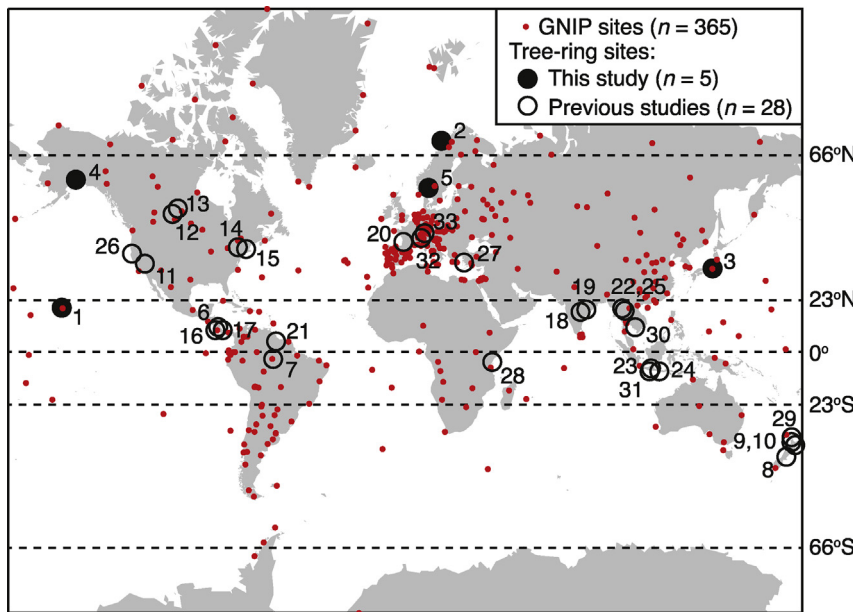


**Fig. 1.** Global distribution of the five tree-ring sites for which we provide new high-resolution  $\delta^{18}\text{O}_{\text{cell}}$  data (closed black circles), augmented by the 28 additional sites (open black circles) for which we include previously published  $\delta^{18}\text{O}_{\text{cell}}$  data. The 33 tree-ring sites are numbered to correspond with the site numbers listed in Table 1. Temperature and precipitation data for each site are included within Table 2. The smaller red circles show the locations of 365 stations accessed from the IAEA GNIP database for precipitation, temperature, and oxygen isotope information (Supplementary Table 3).

**Table 1**  
Tree ring sampling data.

Site no.	Location	Genus	Conifer/angiosperm	No. rings	Reference <sup>a</sup>
1	Mauna Kea, HI, USA; 19.83 °N, 155.60 °W; 2491 m	<i>Sophora</i>	Angiosperm	4	This study <sup>b</sup>
2	Harstad, Norway; 68.84 °N, 16.49 °E; 10 m	<i>Larix</i>	Conifer	4	This study
3	University of Tokyo Tanashi Forest, Tokyo, Japan; 35.73 °N, 139.54 °E; 76 m	<i>Metasequoia</i>	Conifer	4	This study
4	Palmer, AK, USA; 61.48 °N, 149.27 °W; 71 m	<i>Picea</i>	Conifer	4	This study
5	Nordskogen Arboretum, Ås, Norway; 59.67 °N, 10.77 °E; 108 m	<i>Tsuga</i>	Conifer	4	This study
6	Monteverde, Costa Rica; 10.30 °N, 84.80 °E; 1400 m	<i>Ocotea</i>	Angiosperm	10	(Anchukaitis et al., 2008; Fig. 6d)
7	Manaus, Brazil; 3.10 °S, 60.00 °W; 72 m	<i>Tachigali</i>	Angiosperm	3	(Ballantyne et al., 2011; Fig. 3)
8	Balmoral, New Zealand; 42.87 °S, 172.75 °E; 30 m	<i>Pinus</i>	Conifer	2	(Barbour et al., 2002; Fig. 3)
9	Matangi, New Zealand; 37.83 °S, 175.30 °E; 20 m	<i>Pinus</i>	Conifer	2	(Barbour et al., 2002; Fig. 4)
10	Kawerau, New Zealand; 38.17 °S, 176.67 °E; 407 m	<i>Pinus</i>	Conifer	2	(Barbour et al., 2002; Fig. 5)
11	Methuselah Walk, CA, USA; 37.39 °N, 118.18 °W; 3075 m	<i>Pinus</i>	Conifer	35	(Berkelhammer and Stott, 2009; Fig. 2)
12	Prince Albert, Saskatchewan, Canada; 53.22 °N, 105.67 °W; 440 m	<i>Picea</i>	Conifer	20	(Dodd et al., 2008; Fig. 3)
13	East central Saskatchewan, Canada; 54.68 °N, 103.19 °W; 340 m	<i>Larix</i>	Conifer	14	(Dodd et al., 2008; Fig. 4)
14	Green Lake State Park, Fayetteville, NY, USA; 43.05 °N, 75.97 °W; 669 m	<i>Populus</i>	Angiosperm	11	(Dodd et al., 2008; Fig. 5)
15	Harvard Forest, Petersham, MA, USA; 42.48 °N, 72.19 °W; 338 m	<i>Pinus</i>	Conifer	10	(Evans and Schrag, 2004; Fig. 5)
16	Quebrada Grande, Costa Rica; 10.00 °N, 85.00 °W; 300 m	<i>Cordia</i>	Angiosperm	36	(Evans and Schrag, 2004; Fig. 6d)
17	La Selva, Costa Rica; 10.00 °N; 84.00 °W; 40 m	<i>Hyeronima</i>	Angiosperm	17	(Evans and Schrag, 2004; Fig. 7d)
18	Hanamkonda, India; 18.02 °N, 79.57 °E; 224 m	<i>Tectona</i>	Angiosperm	2	(Managave et al., 2010; Fig. 2 AP1)
19	Jagdalpur, India; 19.08 °N, 82.03 °E; 560 m	<i>Tectona</i>	Angiosperm	5	(Managave et al., 2010; Fig. 2 Jag03)
20	Bordeaux, France; 44.72 °N, 0.77 °W; 62 m	<i>Pinus</i>	Conifer	4	(Ogée et al., 2009; Fig. 8)
21	West Pibiri, Guyana; 5.03 °N, 58.62 °W; 73 m	<i>Carapa/Goupi</i>	Angiosperm	63	(Pons and Helle, 2011; Figs. 4–5)
22	Pangmpa, Thailand; 19.57 °N, 98.27 °W; 759 m	<i>Quercus/</i> <i>Miliusa</i>	Angiosperm	67	(Poussart and Schrag, 2005; PG1, PK1)
23	Java, Indonesia; 7.45 °S, 111.55 °E; 68 m	<i>Tectona</i>	Angiosperm	81	(Poussart et al., 2004; Figs. 2–3)
24	Bali, Indonesia; 8.65 °S, 115.22 °E; 32 m	<i>Samanea</i>	Angiosperm	37	(Poussart et al., 2004; Fig. 5 Suar1, Suar3)
25	Chiang Mai, Thailand; 18.5 °N, 98.50 °E; 1455 m	<i>Podocarpus</i>	Conifer	7	(Poussart et al., 2004; Fig. 6)
26	Arcata, CA, USA; 40.88 °N, 124.07 °W; 158 m	<i>Sequoia</i>	Conifer	20	(Roden et al., 2009; Fig. 2)
27	Samos, Greece; 37.70 °N, 26.63 °E; 225 m	<i>Pinus</i>	Conifer	2	(Sarris et al., 2013; Fig. 4b)
28	Gazi Bay, Kenya; 4.42 °S, 39.50 °E; 22 m	<i>Rhizophora</i>	Angiosperm	5	(Verheyden et al., 2004; Fig. 4b)
29	Hamilton, New Zealand; 37.78 °S, 175.28 °E; 20 m	<i>Pinus</i>	Conifer	2	(Wilson and Grinsted, 1978; Fig. 3)
30	Kirirom National Park, Cambodia; 11.29 °N, 104.25 °E; 675 m	<i>Pinus</i>	Conifer	301	(Zhu et al., 2012)
31	Central Java, Indonesia; 7.87 °S, 111.18 °E; 380 m	<i>Tectona</i>	Angiosperm	3	(Schollaen et al., 2013; Fig. 5B)
32	Lötschental, Switzerland; 46.40 °N, 7.75 °E; 1725 m	<i>Larix</i>	Conifer	6	(Treydte et al., 2014; Fig. 2d)
33	Tuttlingen, Germany; 47.98 °N, 8.75 °E; 750 m	<i>Fagus</i>	Angiosperm	5	(Offermann et al., 2011)

<sup>a</sup> Figure numbers refer to those in the listed reference, and do not correspond to figures shown in this study.

<sup>b</sup>  $\delta^{18}\text{O}_{\text{cell}}$  data for the five new sites reported in "this study" are plotted in Fig. 2.

### 3. Results and discussion

#### 3.1. Global dataset of intra-ring oxygen isotope measurements on wood cellulose

Intra-ring  $\delta^{18}\text{O}_{\text{cell}}$  profiles that we produced ( $n = 5$  sites) showed increases and decreases in the  $\delta^{18}\text{O}_{\text{cell}}$  values each growth year with an average amplitude up to  $\sim 4\text{\textperthousand}$  (Fig. 2B,D–G). When comparing the intra-annual  $\delta^{18}\text{O}_{\text{cell}}$  patterns of all 33 sites we noted two distinct patterns. At twelve of the sites (1–2, 9–11, 20, 26–29, 32–33 within Fig. 1, Table 1), the minimum  $\delta^{18}\text{O}_{\text{cell}}$  ( $\delta^{18}\text{O}_{\text{cell(min)}}$ ) value occurred near the ring boundary (transition from latewood to earlywood); at all the other sites,  $\delta^{18}\text{O}_{\text{cell(min)}}$  occurred closer to the middle of each ring. We calculated the intra-annual change in  $\delta^{18}\text{O}_{\text{cell}}$  [ $\Delta(\delta^{18}\text{O}_{\text{cell}})$ ] in tree rings where  $\delta^{18}\text{O}_{\text{cell(min)}}$  occurred near the ring boundary as the average difference between the maximum

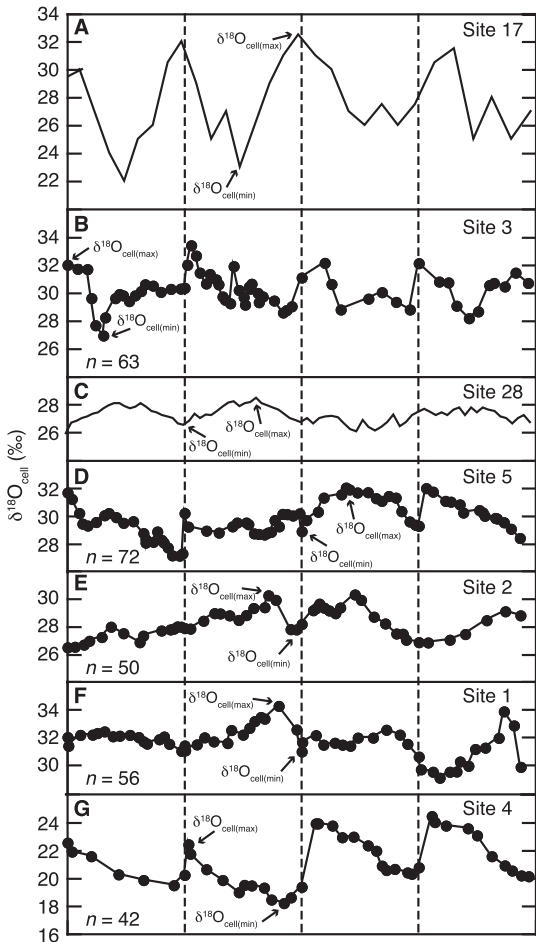


**Fig. 2.** Intra-ring  $\delta^{18}\text{O}_{\text{cell}}$  data for seven of the 33 sites compiled for this study (Table 1, Fig. 1), illustrating the partial range of  $\Delta(\delta^{18}\text{O}_{\text{cell}})$  values observed across the global dataset. Ring boundaries (dashed vertical lines) denote the first earlywood measurement for each ring, separating the data into the four tree-rings depicted; the direction of growth is left to right.  $\Delta(\delta^{18}\text{O}_{\text{cell}})$  values were determined using Eqs. (1A) and (1B) (Table 2); for illustration,  $\delta^{18}\text{O}_{\text{cell(max)}}$  and  $\delta^{18}\text{O}_{\text{cell(min)}}$  for one ring at each site are indicated. The profiles depicted here are arranged in order of increasing  $\Delta(\delta^{18}\text{O}_{\text{cell}})$  value (top to bottom) and show the five sites for which this study reports new  $\delta^{18}\text{O}_{\text{cell}}$  data: (B) Tokyo, Japan (Site 3;  $\Delta(\delta^{18}\text{O}_{\text{cell}}) = -4.3\text{\textperthousand}$ ); (D) Ås, Norway (Site 5;  $\Delta(\delta^{18}\text{O}_{\text{cell}}) = 2.4\text{\textperthousand}$ ); (E) Harstad, Norway (Site 2;  $\Delta(\delta^{18}\text{O}_{\text{cell}}) = 2.4\text{\textperthousand}$ ); (F) Mauna Kea, Hawaii (Site 1;  $\Delta(\delta^{18}\text{O}_{\text{cell}}) = 2.6\text{\textperthousand}$ ); and (G) Palmer, Alaska (Site 4;  $\Delta(\delta^{18}\text{O}_{\text{cell}}) = 3.8\text{\textperthousand}$ ) (data are provided in Supplementary Table 1). Intra-ring data from four of the tree rings from (A) La Selva, Costa Rica (Site 17;  $\Delta(\delta^{18}\text{O}_{\text{cell}}) = -6.4\text{\textperthousand}$ ) and (C) Gazi Bay, Kenya (Site 28;  $\Delta(\delta^{18}\text{O}_{\text{cell}}) = 1.4\text{\textperthousand}$ ) are included to fully visually illustrate the difference between isotopic profiles of varying  $\Delta(\delta^{18}\text{O}_{\text{cell}})$  value. The genus of each tree involved, as well as the number of rings for each of the 33 sites, is specified within Table 1.

( $\delta^{18}\text{O}_{\text{cell(max)}}$ ) and minimum ( $\delta^{18}\text{O}_{\text{cell(min)}}$ )  $\delta^{18}\text{O}_{\text{cell}}$  value within each ring:

$$\Delta(\delta^{18}\text{O}_{\text{cell}}) = \delta^{18}\text{O}_{\text{cell(max)}} - \delta^{18}\text{O}_{\text{cell(min)}}. \quad (1\text{A})$$

In contrast, for rings where  $\delta^{18}\text{O}_{\text{cell(min)}}$  occurred closer to the middle of the ring, we calculated  $\Delta(\delta^{18}\text{O}_{\text{cell}})$  as:

$$\Delta(\delta^{18}\text{O}_{\text{cell}}) = \delta^{18}\text{O}_{\text{cell(min)}} - \delta^{18}\text{O}_{\text{cell(max)}}. \quad (1\text{B})$$

In this way, these two contrasting intra-annual  $\delta^{18}\text{O}_{\text{cell}}$  patterns yielded opposite signs. A list of the  $\delta^{18}\text{O}_{\text{cell(max)}}$ ,  $\delta^{18}\text{O}_{\text{cell(min)}}$ , and  $\Delta(\delta^{18}\text{O}_{\text{cell}})$  values for all tree rings from each of the 33 sites are provided in Supplementary Table 2. Across the full dataset of 33 sites, we saw  $\Delta(\delta^{18}\text{O}_{\text{cell}})$  values range from  $-9.3$  to  $4.0\text{\textperthousand}$  (positive values when  $\delta^{18}\text{O}_{\text{cell(min)}}$  occurred closer to the ring boundary, and negative values when  $\delta^{18}\text{O}_{\text{cell(min)}}$  occurred closer to the middle of the ring) (Table 2) (Fig. 2), leading us to hypothesize that the large range of climate characteristics for these sites might have found expression within the large range of seasonal isotopic profiles we observed. We tested this using a compilation of environmental data that included monthly resolved climate data.

#### 3.2. The relationship between the oxygen isotope values of wood cellulose and meteoric water within a monthly-resolved dataset

Because the oxygen isotope composition of environmental water ( $\delta^{18}\text{O}_{\text{MW}}$ ) is influenced by multiple climate parameters (e.g., Rozanski et al., 1993), many studies have sought to quantify the oxygen isotope relationship between  $\delta^{18}\text{O}_{\text{MW}}$  and plant cellulose ( $\delta^{18}\text{O}_{\text{cell}}$ ) using empirical datasets. However, isotopic exchange occurs during cellulose synthesis (e.g., Luo and Sternberg, 1992; Sternberg et al., 1986) and is specific to the position of oxygen within the glucose moiety (Sternberg et al., 2006, 2007). Three main approaches have been used to search for a universally applicable quantitative relationship between  $\delta^{18}\text{O}_{\text{MW}}$  and  $\delta^{18}\text{O}_{\text{cell}}$ : 1) controlled growth of small plants using water of known isotopic value (e.g., Roden and Ehleringer, 1999; Yakir and DeNiro, 1990); 2) isotopic comparisons between stem cellulose and stem-extracted water from living trees (e.g., Jahren and Sternberg, 2002, 2003); 3) correlation between the  $\delta^{18}\text{O}_{\text{cell}}$  in multiple trees at multiple sites with  $\delta^{18}\text{O}_{\text{MW}}$  values taken from independently compiled datasets, such as the IAEA GNIP database (IAEA/WMO, 2006) (e.g., Sauer et al., 1997; Waterhouse et al., 2002), or calculated values from the Online Isotopes in Precipitation Calculator (OIPC v 2.2) (Bowen, 2013; Bowen et al., 2005) or equations within Bowen and Wilkinson (2002) (e.g., Csank et al., 2013; Richter et al., 2008b). The absolute value of the difference between  $\delta^{18}\text{O}_{\text{MW}}$  and  $\delta^{18}\text{O}_{\text{cell}}$  gained using approaches 1 and 2 (above) have yielded widely disparate values for individual species, suggesting that, for any universally-applicable relationship based on many different plant species, the slope between  $\delta^{18}\text{O}_{\text{cell}}$  and  $\delta^{18}\text{O}_{\text{MW}}$  is not equal to one. Several workers have used approach 3 (above) to show correlations between  $\delta^{18}\text{O}_{\text{cell}}$  and  $\delta^{18}\text{O}_{\text{MW}}$  replete with slope and intercept for conifer, angiosperm, and mixed forest communities. Table 3 shows that such studies yielded slope values of  $0.54$ – $0.89$  across a wide range of geographical locations and plant types.

The high-resolution intra-ring profiles of  $\delta^{18}\text{O}_{\text{cell}}$  that we present here allow us to observe and quantify relative changes in the isotopic composition of cellulose across the growing season. We determined the slope of the relationship between this change in the isotope composition of cellulose [ $\Delta(\delta^{18}\text{O}_{\text{cell}})$ ] and the intra-annual change in the oxygen isotope composition of meteoric water [ $\Delta(\delta^{18}\text{O}_{\text{MW}})$ ] across all of the 33 tree-ring sites (Fig. 3) in order to compare this slope value to the slopes observed for

**Table 2**

Climate and isotope data used to calculate  $\Delta(\delta^{18}\text{O}_{\text{cell}})_{\text{model}}$ ,  $\Delta(\delta^{18}\text{O}_{\text{MW}})_{\text{cell}}$ ,  $\Delta(\delta^{18}\text{O}_{\text{MW}})_{\text{model}}$  for each of the 33 tree-ring sites.

Site no. <sup>a</sup>	Temperature (°C)		Precipitation (mm) <sup>c</sup>		$\Delta(\delta^{18}\text{O}_{\text{cell}})^{\text{d}}$ (%)	$\Delta(\delta^{18}\text{O}_{\text{cell}})_{\text{model}}^{\text{e}}$ (%)	$\Delta(\delta^{18}\text{O}_{\text{MW}})^{\text{f}}$ (%)	$\Delta(\delta^{18}\text{O}_{\text{MW}})_{\text{cell}}^{\text{g}}$ (%)	$\Delta(\delta^{18}\text{O}_{\text{MW}})_{\text{model}}^{\text{h}}$ (%)
	$T_{\text{max}}$	$T_{\text{min}}^{\text{b}}$	$P_{\text{summer}}$	$P_{\text{winter}}$					
1	15.5	11.6	146	256	2.6 ± 1.7	1.5	4.3	4.0	2.2
2	14.0	0.0	373	476	2.4 ± 0.7	4.1	6.0	3.6	6.2
3	26.5	3.2	1091	424	-4.3 ± 0.8	1.4	2.6	-6.5	2.2
4	14.7	0.0	264	107	3.8 ± 0.6	2.8	6.7	5.8	4.3
5	17.5	0.0	462	301	2.4 ± 2.7	3.4	4.4	3.6	5.1
6	19.2	17.2	2055	630	-6.1 ± 1.0	-7.3	-7.3	-9.2	-11.1
7	27.6	26.0	1562	724	-5.0 ± 1.0	-4.3	-5.1	-7.6	-6.5
8	19.8	10.8	343	248	0.0 ± 5.7	1.4	2.5	0.0	2.1
9	18.5	9.0	490	628	3.5 ± 0.7	2.8	2.4	5.3	4.3
10	19.3	9.8	455	900	4.0 ± 1.4	4.5	2.1	6.1	6.8
11	6.9	0.0	61	184	2.7 ± 1.3	2.5	5.4	4.1	3.8
12	17.5	0.0	319	106	2.2 ± 0.9	3.1	5.2	3.3	4.7
13	18.5	0.0	345	118	1.8 ± 0.9	3.2	5.3	2.8	4.9
14	21.9	0.0	534	446	2.0 ± 0.6	4.6	6.1	3.1	7.0
15	20.6	0.0	694	528	3.9 ± 3.0	4.0	5.6	5.8	6.0
16	24.5	23.0	1600	200	-4.4 ± 1.1	-7.3	-8.1	-6.6	-11.1
17	27.0	24.0	2830	1685	-6.4 ± 2.4	-5.7	-7.8	-9.7	-8.6
18	34.0	22.5	865	75	-4.6 ± 2.1	-2.4	-9.3	-7.0	-3.6
19	31.0	20.0	1410	120	-5.4 ± 1.3	-5.1	-8.7	-8.2	-7.7
20	22.8	6.5	413	445	3.9 ± 1.9	3.7	3.7	6.0	5.6
21	27.0	26.0	1625	1135	-2.3 ± 1.5	-2.5	-3.4	-3.5	-3.8
22	30.0	22.0	1144	117	-3.9 ± 1.4	-4.2	-5.7	-5.9	-6.3
23	26.5	25.0	1660	380	-3.3 ± 1.5	-6.7	-2.5	-5.0	-10.1
24	29.6	26.1	1396	336	-2.6 ± 1.6	-5.2	-2.1	-3.9	-7.8
25	27.7	20.0	1592	174	-9.3 ± 4.9	-6.3	-4.6	-14.1	-9.6
26	14.0	9.0	153	815	1.7 ± 0.5	4.7	4.4	2.5	7.2
27	27.5	10.0	95	488	3.4 ± 1.3	5.6	3.5	5.2	8.6
28	29.9	23.3	410	680	1.4 ± 0.3	2.2	2.5	2.1	3.4
29	18.5	9.0	526	662	2.5 ± 0.5	2.8	2.5	3.8	4.3
30	29.8	25.8	1145	290	-4.0 ± NA	-4.0	-3.9	-6.1	-6.0
31	26.5	25.5	1480	415	-4.6 ± 1.2	-5.6	-2.7	-7.0	-8.5
32	16.7	0.0	556	453	4.1 ± 1.3	3.5	6.1	6.2	5.3
33	17.1	0.0	556	425	3.0 ± NA	3.5	5.4	4.5	5.3

<sup>a</sup> See Table 1 and Fig. 1.

<sup>b</sup> Because growth of new wood may stop or slow considerably when temperatures fall below freezing, we set  $T_{\text{min}} = 0$  °C for sites with average monthly temperatures that fell below 0 °C, which follows the protocols of Bowen et al. (2005).

<sup>c</sup>  $P_{\text{summer}}$  and  $P_{\text{winter}}$  are the average total summer and winter precipitation, respectively (mm), where winter and summer were defined as 6-month periods (November through April or May through October) based on whether sites were in the northern or southern hemispheres.

<sup>d</sup> Calculated using Eqs. (1A or 1B) from high-resolution, intra-ring  $\delta^{18}\text{O}_{\text{cell}}$  measurements. Reported as the average  $\pm 1\sigma$ .

<sup>e</sup> Calculated using Eq. (8) with  $A = 0.0082$ ,  $M = 0.66$ , and the  $T_{\text{max}}$ ,  $T_{\text{min}}$ ,  $P_{\text{summer}}$ , and  $P_{\text{winter}}$  values presented in this table.

<sup>f</sup> Calculated using Eqs. (2A or 2B) with long-term average monthly data from the IAEA-GNIP database or OIPC (v. 2.2) tool for months with average temperatures  $>0$  °C.

<sup>g</sup> Calculated using Eq. (3) with  $M = 0.66$  and the  $\Delta(\delta^{18}\text{O}_{\text{cell}})$  values presented in this table.

<sup>h</sup> Calculated using Eq. (7) with  $A = 0.0082$  and the  $T_{\text{max}}$ ,  $T_{\text{min}}$ ,  $P_{\text{summer}}$ , and  $P_{\text{winter}}$  values presented in this table.

relationships between absolute  $\delta^{18}\text{O}$  cellulose and meteoric water values (Table 3). To be consistent with calculated seasonal changes in  $\delta^{18}\text{O}_{\text{cell}}$  [ $\Delta(\delta^{18}\text{O}_{\text{cell}})$ ; Eqs. (1A) and (1B)], we defined  $\Delta(\delta^{18}\text{O}_{\text{MW}})$  values as the average difference between the maximum ( $\delta^{18}\text{O}_{\text{MW(max)}}$ ) and minimum ( $\delta^{18}\text{O}_{\text{MW(min)}}$ ) monthly  $\delta^{18}\text{O}_{\text{MW}}$  values:

$$\Delta(\delta^{18}\text{O}_{\text{MW}}) = \delta^{18}\text{O}_{\text{MW(max)}} - \delta^{18}\text{O}_{\text{MW(min)}} \quad (2\text{A})$$

or

$$\Delta(\delta^{18}\text{O}_{\text{MW}}) = \delta^{18}\text{O}_{\text{MW(min)}} - \delta^{18}\text{O}_{\text{MW(max)}}. \quad (2\text{B})$$

**Table 3**

Oxygen isotope relationships between meteoric water and tree-ring cellulose [ $\delta^{18}\text{O}_{\text{cell}} = (\text{slope})(\delta^{18}\text{O}_{\text{MW}}) + \text{intercept}$ ].

Plant type(s)	Slope	Intercept (%)	$R^2$	Reference
<i>Correlation between <math>\delta^{18}\text{O}_{\text{MW}}</math> and <math>\delta^{18}\text{O}_{\text{cell}}</math></i> <sup>a</sup>				
Conifers and angiosperms (all data)	0.61	32.4	0.54	Sternberg et al. (2007)
Conifers and angiosperms (excludes Tucson, AZ)	0.60	31.9	0.58	Sternberg et al. (2007)
Conifers and angiosperms (excludes Sugarloaf Key, FL)	0.89	35.4	0.78	Sternberg et al. (2007)
Conifers and angiosperms	0.61	33.2	0.70	Csank et al. (2013)
Angiosperms	0.54	33.1	0.75	Richter et al. (2008b)
Conifers	0.59	35.1	0.90	Richter et al. (2008b)
<i>Fagus sylvatica</i>	0.76 ± 0.15	Not reported	0.55	Saurer et al. (1997)
<i>Quercus robur</i>	0.59	33.4	0.67	Waterhouse et al. (2002)
<i>Correlation between <math>\Delta(\delta^{18}\text{O}_{\text{MW}})</math> and <math>\Delta(\delta^{18}\text{O}_{\text{cell}})</math> (data plotted in Fig. 3)</i>				
Conifers and angiosperms	0.66	0.0	0.74	This study

<sup>a</sup> When  $\delta^{18}\text{O}_{\text{MW}}$  data were not provided,  $\delta^{18}\text{O}_{\text{MW}}$  values were calculated from measurements of the  $\delta^{18}\text{O}$  value of stem water ( $\delta^{18}\text{O}_{\text{SW}}$ ) using the following equation from Fig. 1 within Sternberg et al. (2007):  $\delta^{18}\text{O}_{\text{MW}} = (\delta^{18}\text{O}_{\text{SW}} - 0.55)/1.15$ .

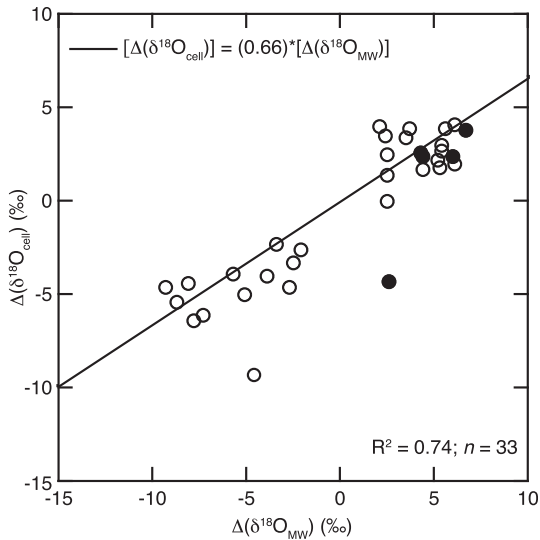


**Fig. 3.** Seasonal changes in the oxygen isotope composition profile of cellulose [ $\Delta(\delta^{18}\text{O}_{\text{cell}})$ ] measured for all 33 tree-ring sites (Table 1) plotted against  $\Delta(\delta^{18}\text{O}_{\text{MW}})$  determined using Eqs. (2A) and (2B) (Table 2). The relationship results in a slope ( $M = 0.66$ ) that is within the range of slope values (0.54–0.76) reported for comparisons between whole-ring  $\delta^{18}\text{O}_{\text{cell}}$  and  $\delta^{18}\text{O}_{\text{MW}}$  for diverse species (Table 3). Closed circles represent the five new tree-ring sites; open circles represent the 28 published tree-ring sites.

Eq. (2A) was used for sites where  $\delta^{18}\text{O}_{\text{MW(min)}}$  values occurred in winter (Northern Hemisphere: November through April; Southern Hemisphere: May through October), and Eq. (2B) was used for sites where  $\delta^{18}\text{O}_{\text{MW(min)}}$  occurred in summer months (Northern Hemisphere: May through October; Southern Hemisphere: November through April). Thus, calculated  $\Delta(\delta^{18}\text{O}_{\text{MW}})$  values were positive when  $\delta^{18}\text{O}_{\text{MW(min)}}$  occurred during winter (Eq. (2A)) and negative when  $\delta^{18}\text{O}_{\text{MW(min)}}$  occurred during summer (Eq. (2B)). This differs from publications such as Bowen (2008), which calculated  $\Delta(\delta^{18}\text{O}_{\text{MW}})$  using Eq. (2A) for all sites, thus exclusively generating values  $>0\text{\textperthousand}$ . In our analysis the sign of the  $\Delta(\delta^{18}\text{O}_{\text{MW}})$  value indicates the season of maximum (and minimum)  $\delta^{18}\text{O}_{\text{MW}}$  value, and thus differentiates sites in which temperature and  $\delta^{18}\text{O}_{\text{MW}}$  value are positively *versus* negatively correlated.  $\Delta(\delta^{18}\text{O}_{\text{MW}})$  values were calculated using the monthly  $\delta^{18}\text{O}_{\text{MW}}$  data available for each site from the IAEA GNIP month-by-month database (IAEA/WMO, 2006) (Table 2). For samples from trees not located at GNIP sampling sites, we used  $\Delta(\delta^{18}\text{O}_{\text{MW}})$  values generated by the Online Isotopes in Precipitation Calculator (OIPC v 2.2) (Bowen, 2013), a tool created by Bowen and Ravennaugh (2003) and Bowen et al. (2005) that yields spatially-interpolated  $\delta^{18}\text{O}_{\text{MW}}$  values from the GNIP database. The data used to calculate  $\Delta(\delta^{18}\text{O}_{\text{MW}})$  values for comparison with tree-ring records were restricted to months with average temperatures  $>0\text{ }^{\circ}\text{C}$  (i.e., “growing-season” months), in order to be consistent with the protocols described within Bowen et al. (2005).

For our dataset of intra-ring profiles from 33 sites, we found a slope ( $M$ ) = 0.66 with an associated  $R^2 = 0.74$  for the relationship between  $\Delta(\delta^{18}\text{O}_{\text{MW}})$  calculated using Eqs. (2A) and (2B) and  $\Delta(\delta^{18}\text{O}_{\text{cell}})$  calculated using Eqs. (1A) and (1B) (Fig. 3). This slope value falls within the range of slopes based on whole-ring  $\delta^{18}\text{O}_{\text{cell}}$  measurements (0.54–0.89; Table 3), and the slope value of 0.73 determined from whole-ring  $\delta^{18}\text{O}$  measurements of cellulose-derived phenylglucosazone (Sternberg et al., 2007). Based on the scale of our dataset, we propose that intra-ring cellulose profiles can be used to estimate the average intra-annual change in  $\delta^{18}\text{O}_{\text{MW}}$  using the following equation:

$$\Delta(\delta^{18}\text{O}_{\text{MW}}) = \Delta(\delta^{18}\text{O}_{\text{cell}}) / 0.66. \quad (3)$$

By studying relative changes in  $\delta^{18}\text{O}$ , rather than absolute  $\delta^{18}\text{O}$  values, we avoid issues arising from differences in leaf-water enrichment and transpiration among individual trees (e.g., Gessler et al., 2013), allowing us to also compare diverse species that may otherwise have different intercept values (for example, see Table 3) even when growing under the same conditions. Our measured  $\Delta(\delta^{18}\text{O}_{\text{cell}})$  values, which ranged from  $-9.4$  to  $4.0\text{\textperthousand}$  for all sites, yielded estimates of  $\Delta(\delta^{18}\text{O}_{\text{MW}})$  values ranging from  $-14.1$  to  $6.1\text{\textperthousand}$  via Eq. (3) (Table 2). These cellulose-generated  $\Delta(\delta^{18}\text{O}_{\text{MW}})$  estimates determined using Eq. (3) are hereafter described as “ $\Delta(\delta^{18}\text{O}_{\text{MW}})_{\text{cell}}$ ”.

### 3.3. Global dataset of seasonal climate and the intra-annual change in the oxygen isotope composition of meteoric water

We have quantified above how measurements of  $\Delta(\delta^{18}\text{O}_{\text{cell}})$  can be used to generate accurate estimates of  $\Delta(\delta^{18}\text{O}_{\text{MW}})$ . Such estimates would be extremely useful in paleoclimate reconstruction, if they could be shown to correlate with meaningful climate characteristics. Empirical datasets suggest that both temperature and precipitation amount exert an influence on the isotopic composition of the resultant rainfall (e.g., Araguás-Araguás et al., 1998; Bowen, 2008; Craig, 1961; Dansgaard, 1964; Gat and Matsui, 1991; Njitchoua et al., 1999; Rozanski et al., 1992, 1993). In order to quantitatively evaluate the potential for  $\Delta(\delta^{18}\text{O}_{\text{MW}})$  to accurately predict these two climate parameters, we compiled the average precipitation (mm), temperature ( $^{\circ}\text{C}$ ), and  $\delta^{18}\text{O}_{\text{MW}}$  value for each month of the year at the 365 globally distributed GNIP sites pictured in Fig. 1, using the GNIP month-by-month database (IAEA/WMO, 2006), as above. Although the database contains more than 900 sites, we limited our analysis to the 365 stations that reported sufficient data for the calculation of  $T_{\min}$ ,  $T_{\max}$ ,  $P_{\text{winter}}$ ,  $P_{\text{summer}}$ , and  $\Delta(\delta^{18}\text{O}_{\text{MW}})$ , where  $T_{\min}$  is the average cold month mean temperature ( $^{\circ}\text{C}$ ),  $T_{\max}$  is the average warm month mean temperature ( $^{\circ}\text{C}$ ), and  $P_{\text{winter}}$  and  $P_{\text{summer}}$  are the average total winter and summer precipitation (mm), respectively, where winter and summer were defined as 6-month periods (November through April or May through October) based on whether sites were in the northern or southern hemispheres. As previously,  $\Delta(\delta^{18}\text{O}_{\text{MW}})$  is the average difference between the maximum ( $\delta^{18}\text{O}_{\text{MW(max)}}$ ,  $\text{\textperthousand}$ ) and minimum ( $\delta^{18}\text{O}_{\text{MW(min)}}$ ,  $\text{\textperthousand}$ ) values (Eqs. (2A) and (2B)), but here data were not restricted to only growing season months with average temperatures  $>0\text{ }^{\circ}\text{C}$ . A list of the 365 sites and the calculated  $T_{\min}$ ,  $T_{\max}$ ,  $P_{\text{winter}}$ ,  $P_{\text{summer}}$ , and  $\Delta(\delta^{18}\text{O}_{\text{MW}})$  data are provided in Supplementary Table 3. These sites, which span  $158^{\circ}$  of latitude, represent a wide range of seasonal climates, from tropical environments near the equator where the intra-annual change in temperature ( $T_{\max} - T_{\min}$ ) is  $<1\text{ }^{\circ}\text{C}$  (e.g., Truk Island and Yap Island, Federated States of Micronesia; Canton Island and Tarawa Island, Republic of Kiribati; Madang, Papua New Guinea; Jayapura, Indonesia; and Esmeraldas, Ecuador) to sites within continental interiors where  $T_{\max} - T_{\min} > 40\text{ }^{\circ}\text{C}$  (e.g., Ulaanbaatar, Mongolia and Hall Beach, Nunavut, Canada). Similarly, seasonal changes in precipitation ( $P_{\text{winter}} - P_{\text{summer}}$ ) ranged across the sites from Mediterranean climates with  $P_{\text{winter}} - P_{\text{summer}} > 500\text{ mm}$  (e.g., Antalya, Turkey; Perth, Australia; Penhas Douradas, Portugal) to monsoon climates with  $P_{\text{winter}} - P_{\text{summer}} < -1500\text{ mm}$  (e.g., Manila, Philippines; Hong Kong; Darwin, Northern Territory, Australia; San Salvador (Ilopango), El Salvador; and Shillong, India). Based on this, we argue that a relationship developed upon this large range in climate characteristics can be considered to robustly include the entire range of possible climates presently found on Earth.

Maximum monthly  $\delta^{18}\text{O}_{\text{MW}}$  values ( $\delta^{18}\text{O}_{\text{MW(month)}}$ ) occurred during summer for 279 out of the 365 sites (76%), consistent with the strong positive relationship between temperature and  $\delta^{18}\text{O}_{\text{MW}}$  classically suggested (e.g., [Dansgaard, 1964](#)). Overall,  $\Delta(\delta^{18}\text{O}_{\text{MW}})$  values ranged from  $<-10.0\text{\textperthousand}$  (e.g., Hanoi, Vietnam and Shillong, India) to  $>20.0\text{\textperthousand}$  (Hall Beach and Pond Inlet, Nunavut, Canada; Inuvik, Northwest Territories, Canada; and Ulaanbaatar, Mongolia);  $\Delta(\delta^{18}\text{O}_{\text{MW}})$  generally increased with increasing distance from the equator ( $R^2 = 0.48$ ,  $P < 0.001$ ). The highest and lowest  $\Delta(\delta^{18}\text{O}_{\text{MW}})$  values were found within high-latitude continental interiors (e.g., Canada and Siberia) and low latitude monsoon regions (e.g., Southeast Asia, Central America, and South America), respectively ([Supplementary Table 3](#)). We noted no correlation between  $\Delta(\delta^{18}\text{O}_{\text{MW}})$  and the average annual amount-weighted oxygen isotope value of meteoric water ( $R^2 = 0.02$ ), indicating that mean-annual and seasonal values yield different isotopic information.

### 3.4. The relationship between temperature and oxygen isotopes in meteoric water within a monthly-resolved dataset

In order to discover a relationship between environmental temperature and the oxygen isotope composition of precipitation applicable to diverse climates across the planet, we plotted  $\delta^{18}\text{O}_{\text{MW(month)}}$  values against the corresponding average monthly temperature ( $T_{\text{month}}$ ) for each of the 365 sites discussed above ([Fig. 4](#)). The resulting relationship followed a hyperbolic relationship across a very large range in temperature ( $-39.8 \leq T_{\text{month}} \leq 33.4^\circ\text{C}$ ):

$$\delta^{18}\text{O}_{\text{MW(month)-hyper}}} = [(17.57T_{\text{month}})/(39.89 + 0.44T_{\text{month}})] - 12.33 \quad (4)$$

with  $R = 0.80$  ( $n = 4312$ ) ([Fig. 4](#)). Our choice of fit as a hyperbolic rather than linear relationship is consistent with the early observation by [Dansgaard \(1964\)](#) that curve-fit  $\delta^{18}\text{O}_{\text{MW}}$  values should not exceed  $0\text{\textperthousand}$ , except under highly evaporative conditions. Eq. (4) produces monthly  $\delta^{18}\text{O}_{\text{MW}}$  values calculated from the best-fit hyperbolic function ( $\delta^{18}\text{O}_{\text{MW(month)-hyper}}}$ ) that are  $>0\text{\textperthousand}$  only for  $T_{\text{month}} > 40^\circ\text{C}$ , average monthly temperatures higher than those found anywhere on Earth ([New et al., 2002](#)).

Previous analyses of the dependence of the oxygen isotope composition of meteoric water on environmental temperature have been performed using a regional dataset of mean annual values

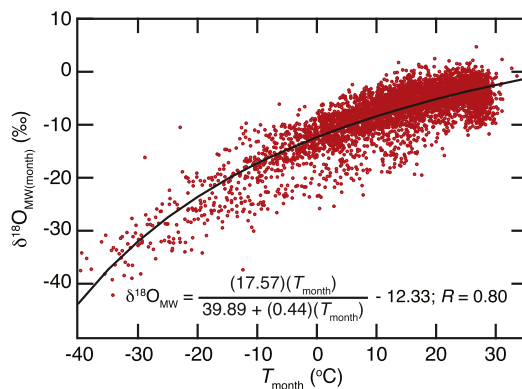


**Fig. 4.** The effect of temperature on  $\delta^{18}\text{O}_{\text{MW}}$ . The long-term average value for each month of the year ( $\delta^{18}\text{O}_{\text{MW(month)}}$ ,  $\text{\textperthousand}$ ) is plotted against the long-term average temperature ( $T_{\text{month}}$ ,  $^\circ\text{C}$ ) for the same month at the same site. Up to twelve monthly averages were calculated for each of the 365 sites pictured in [Fig. 1](#) ( $n = 4312$ ). The black curve represents a best-fit hyperbolic relationship through the red data ( $r = 0.80$ ; Eq. (4)).

([Dansgaard, 1964](#); [Jouzel et al., 1997](#); [Rozanski et al., 1992](#)), or a global dataset of sub-annual values at individual stations ([Bowen, 2008](#)) or across spatially distributed sites ([Fricke and O'Neil, 1999](#)). These analyses produced constant  $\delta^{18}\text{O}_{\text{MW}}/T$  gradient values ( $\text{\textperthousand}/^\circ\text{C}$ ) from linear regressions fit through temperature and  $\delta^{18}\text{O}_{\text{MW}}$  data. In contrast, our non-linear relationship developed across the entire range of global temperature suggests that the  $\delta^{18}\text{O}_{\text{MW}}/T$  gradient is not constant, but changes as a function of temperature, consistent with observations made by [Rozanski et al. \(1993\)](#). In order to quantify this, we calculated the  $\delta^{18}\text{O}_{\text{MW}}/T$  gradient as the first derivative of Eq. (4):

$$\delta^{18}\text{O}_{\text{MW}}/T \text{ gradient} (\text{\textperthousand}/^\circ\text{C}) = 701.01/(39.89 + 0.44T_{\text{month}})^2. \quad (5)$$

Eq. (5) thus calculates the  $\delta^{18}\text{O}_{\text{MW}}/T$  gradient as a continuous function of temperature and is based on a global dataset of average monthly values. This determination of gradient as a function of temperature is consistent with previous analyses that produced constant gradient values across limited temperature ranges. For example, the average gradient calculated using Eq. (5) for cold months (i.e.,  $T_{\text{month}} < 0^\circ\text{C}$ ) is  $0.59 \pm 0.18\text{\textperthousand}/^\circ\text{C}$  (mean  $\pm 1\sigma$ ;  $n = 602$ ), which is very similar to gradients observed by [Dansgaard \(1964\)](#) and [Jouzel et al. \(1997\)](#) ( $0.695$  and  $0.64\text{\textperthousand}/^\circ\text{C}$ , respectively) for sites with sub-freezing mean annual temperature (MAT). In addition, [Bowen \(2008\)](#) found that calculated gradients varied among sites, especially when comparing high versus low-latitude sites. The same study calculated an average gradient of  $0.30 \pm 0.10\text{\textperthousand}/^\circ\text{C}$  (mean  $\pm 1\sigma$ ) for sites with statistically significant linear correlations ( $n = 212$ ), which is consistent with the average gradient of  $0.36 \pm 0.12\text{\textperthousand}/^\circ\text{C}$  (mean  $\pm 1\sigma$ ) calculated using Eq. (5) ( $n = 4372$ ). [Fricke and O'Neil \(1999\)](#) determined gradients of  $0.67$ ,  $0.58$ , and  $0.42\text{\textperthousand}/^\circ\text{C}$  using polar winter, mid-latitude winter, and mid-latitude summer data, respectively. This decrease in gradient with increasing temperature is consistent with the trends observed with Eq. (5). Thus we use the single hyperbolic equation (Eq. (4)) to describe the dependence of temperature on  $\delta^{18}\text{O}_{\text{MW}}$ ; this equation is consistent with and reconciles the previously published linear gradient values obtained from diverse datasets.

The above analysis implies that using only monthly temperature data from the GNIP database, Eq. (4) allows us to quantify the oxygen isotope composition of meteoric water for any month of the year. As an extension of this, we can use monthly temperature data to quantify the average intra-annual change in  $\delta^{18}\text{O}_{\text{MW}}$  [ $\Delta(\delta^{18}\text{O}_{\text{MW}})$ ] as the difference between  $\delta^{18}\text{O}_{\text{MW}}$  values determined at  $T_{\text{max}}$  and  $T_{\text{min}}$  using Eq. (4):

$$\Delta(\delta^{18}\text{O}_{\text{MW}}) = [(17.57T_{\text{max}})/(39.89 + 0.44T_{\text{max}})] - [(17.57T_{\text{min}})/(39.89 + 0.44T_{\text{min}})]. \quad (6)$$

$\Delta(\delta^{18}\text{O}_{\text{MW}})$  values produced using Eq. (6) (hereafter known as " $\Delta(\delta^{18}\text{O}_{\text{MW}})_T$ ") for the 365 sites are listed in [Supplementary Table 3](#). These data suggest that at warm sites, changes in temperature have less effect on seasonal ranges in  $\delta^{18}\text{O}_{\text{MW}}$  than at cooler sites, as predicted from [Fig. 4](#). For example, the difference between  $T_{\text{max}}$  and  $T_{\text{min}}$  in New Delhi, India (a warm site with  $T_{\text{max}} = 33.4^\circ\text{C}$  and  $T_{\text{min}} = 14.1^\circ\text{C}$ ) and Scoresbysund, Greenland (a cool site with  $T_{\text{max}} = 2.8^\circ\text{C}$  and  $T_{\text{min}} = -16.6^\circ\text{C}$ ) are nearly identical ( $T_{\text{max}} - T_{\text{min}} = 19.3$  and  $19.4^\circ\text{C}$ , respectively), but Eq. (6) produces very different values of  $\Delta(\delta^{18}\text{O}_{\text{MW}})_T$  for the two sites ( $\Delta(\delta^{18}\text{O}_{\text{MW}})_T = 5.4$  and  $10.1\text{\textperthousand}$  for New Delhi and Scoresbysund, respectively). We note that at Scoresbysund, a site without a significant wet season, the value of  $\Delta(\delta^{18}\text{O}_{\text{MW}})_T$  generated by Eq. (6) ( $10.1\text{\textperthousand}$ ) closely approximates the  $\Delta(\delta^{18}\text{O}_{\text{MW}})$  value generated

from the GNIP database (9.4‰). In contrast, for New Delhi, which has a highly seasonal precipitation regime, the value of  $\Delta(\delta^{18}\text{O}_{\text{MW}})$  generated by Eq. (6) (5.4‰) is very different from the  $\Delta(\delta^{18}\text{O}_{\text{MW}})$  value generated from the GNIP database (−9.0‰). For sites like New Delhi, the effect of the extreme differences in precipitation amount must be taken into account in order to accurately predict  $\Delta(\delta^{18}\text{O}_{\text{MW}})$  value using temperature information.

### 3.5. Incorporating the effects of precipitation amount on oxygen isotopes in meteoric water

On a global scale, a pattern emerged for the discrepancies between the intra-annual change in  $\delta^{18}\text{O}_{\text{MW}}$  gained from average monthly measured values in the GNIP database [ $\Delta(\delta^{18}\text{O}_{\text{MW}})$ ] and estimates based only on temperature [ $\Delta(\delta^{18}\text{O}_{\text{MW}})_T$ ]. While  $\Delta(\delta^{18}\text{O}_{\text{MW}})_T$  was calculated as being >0‰ for all 365 sites (Supplementary Table 3), nearly a quarter of the sites ( $n = 86$ ) have  $\Delta(\delta^{18}\text{O}_{\text{MW}})$  values <0‰ (i.e.,  $\delta^{18}\text{O}_{\text{MW(min)}}$ ) occurring in summer months; Eq. (2B) (Fig. 5). Most (76%) of these sites with  $\Delta(\delta^{18}\text{O}_{\text{MW}}) < 0\text{‰}$  were located in the tropics, and all of them were located within 37° north or south of the equator (Fig. 5B). Fig. 6 shows that the highest absolute discrepancies between summer and winter rainfall ( $|P_{\text{winter}} - P_{\text{summer}}|$ ) occur in the tropics. Multiple authors have described how heavy precipitation amount leads to lower  $\delta^{18}\text{O}_{\text{MW}}$  values (Araguás-Araguás et al., 1998; Bowen, 2008; Dansgaard, 1964; Rozanski et al., 1993). As a result, multiple studies have observed annual lows in  $\delta^{18}\text{O}_{\text{MW}}$  during the summer rainy season at tropical sites (e.g., Araguás-Araguás et al., 1998; Dayem et al., 2010; Gonfiantini et al., 2001; Xie et al., 2011). Based on this, we hypothesize that at low latitudes, the minimum values of  $\delta^{18}\text{O}_{\text{MW(month)}}$  occurred during the summer as a product of very rainy summers combined with relatively smaller temperature changes between seasons. In order to add the precipitation amount effect to the calculation of  $\Delta(\delta^{18}\text{O}_{\text{MW}})$  within Eq. (6), we inserted a term that scales the influence of ( $P_{\text{winter}} - P_{\text{summer}}$ ) by a positive constant ( $A$ ):

$$\Delta(\delta^{18}\text{O}_{\text{MW}})_{\text{model}} = [(17.57T_{\text{max}})/(39.89 + 0.44T_{\text{max}})] - [(17.57T_{\text{min}})/(39.89 + 0.44T_{\text{min}})] + A(P_{\text{winter}} - P_{\text{summer}}). \quad (7)$$

Eq. (7) models the intra-annual change in  $\delta^{18}\text{O}_{\text{MW}}$  using seasonal climate parameters of both temperature and precipitation [ $\Delta(\delta^{18}\text{O}_{\text{MW}})_{\text{model}}$ ]. The equation is structured such that an increase in winter precipitation relative to summer precipitation will yield greater  $\Delta(\delta^{18}\text{O}_{\text{MW}})_{\text{model}}$  values and vice-versa. Such an equation could be useful for the calculation of paleotemperature and/or paleoseasonality under scenarios where fossil cellulose is available for analysis. In order to determine the best value of  $A$ , we used GNIP database values for  $T_{\text{max}}$ ,  $T_{\text{min}}$ ,  $P_{\text{winter}}$ ,  $P_{\text{summer}}$ , and  $\Delta(\delta^{18}\text{O}_{\text{MW}})$  at each of the 365 sites listed (Supplementary Table 3) and shown on Fig. 1. We iteratively minimized the sum of the residuals squared [ $(\Delta(\delta^{18}\text{O}_{\text{MW}}) - \Delta(\delta^{18}\text{O}_{\text{MW}})_{\text{model}})^2$ ] using Eq. (7); this optimization yielded  $A = 0.0082$  with  $R^2 = 0.68$  for the 1:1 line  $\Delta(\delta^{18}\text{O}_{\text{MW}}) = \Delta(\delta^{18}\text{O}_{\text{MW}})_{\text{model}}$  (Fig. 7). Thus our analysis of the GNIP database revealed that a 100 mm increase or decrease in the balance between  $P_{\text{winter}}$  and  $P_{\text{summer}}$  changes  $\Delta(\delta^{18}\text{O}_{\text{MW}})_{\text{model}}$  by 0.82‰.

The  $\delta^{18}\text{O}_{\text{MW}}$  depletion rate we determined here ( $A = 0.0082\text{‰}/\text{mm}$ ) is somewhat lower than rates reported from other studies [e.g.,  $0.0198 \pm 0.0115\text{‰}/\text{mm}$ , Bowen (2008);  $0.0178$  and  $0.019\text{‰}/\text{mm}$ , Jouzel et al. (1997);  $0.0124\text{‰}/\text{mm}$ , Lachniet and Patterson (2009)]. Our lower rate likely results from our inclusion of all 365 sites in our analysis, whereas these previous studies focused only

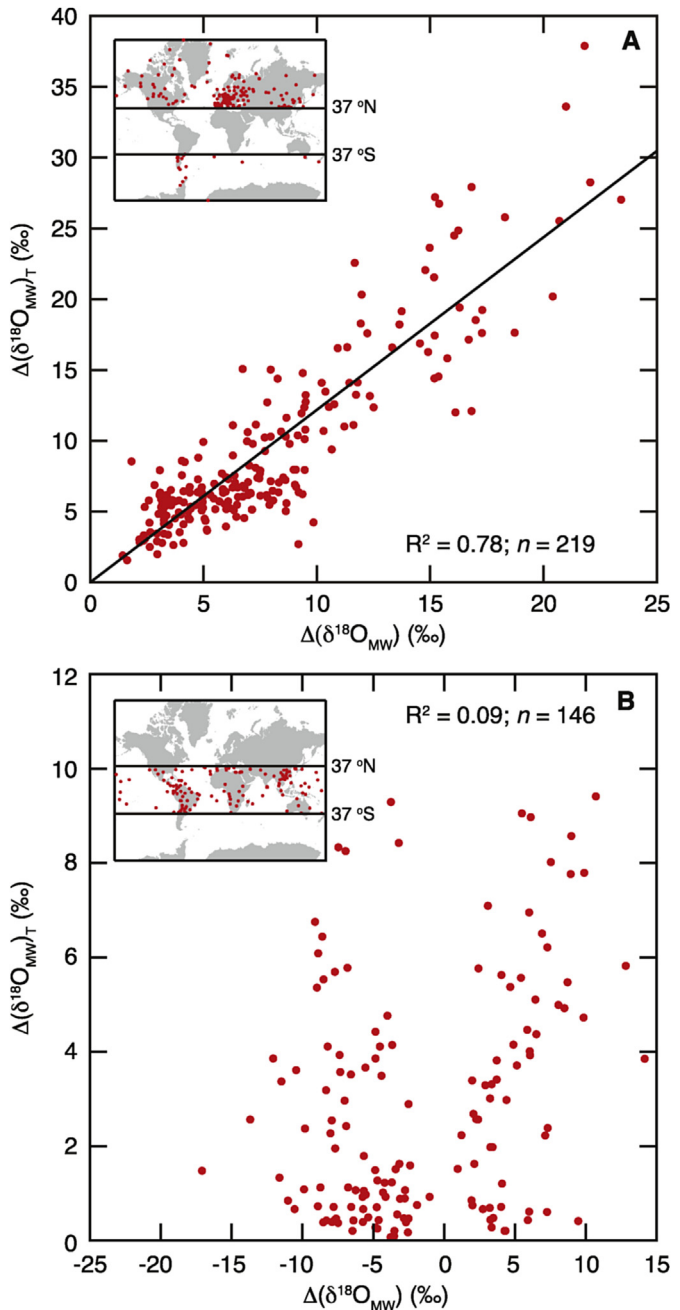


**Fig. 5.** Correlation between the seasonal change in the oxygen isotopes in meteoric water, as determined from the GNIP database [ $\Delta(\delta^{18}\text{O}_{\text{MW}})$ ], versus calculations based only on changes in temperature [ $\Delta(\delta^{18}\text{O}_{\text{MW}})_T$ ] using Eq. (6). Data were separated into (A) high-latitude ( $>37^\circ$  north or south of the equator) and (B) low-latitude ( $<37^\circ$  north or south of the equator) sites to illustrate that seasonal changes in  $\delta^{18}\text{O}_{\text{MW}}$  are strongly controlled by temperature at high-latitude sites ( $R^2 = 0.78$ ), but not at low-latitude sites ( $R^2 = 0.09$ ).

on sites with significant isotope–precipitation relationships (Bowen, 2008), tropical and monsoonal regions with strong changes in seasonal precipitation (Jouzel et al., 1997), or sites within a small geographic region (Lachniet and Patterson, 2009). As shown in Bowen (2008), middle to high latitude sites, which are well-represented in our dataset (Fig. 1), display an inverse relationship between precipitation amount and  $\delta^{18}\text{O}_{\text{MW}}$  that results from the temperature effect dominating the  $\delta^{18}\text{O}_{\text{MW}}$  signal at these sites. Inclusion of these temperature-dominated sites in our analysis

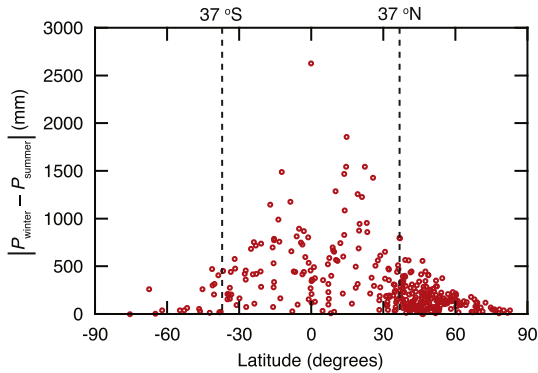


**Fig. 6.** Seasonal precipitation data calculated as the absolute difference between summer ( $P_{\text{summer}}$ ) and winter ( $P_{\text{winter}}$ ) precipitation ( $|P_{\text{winter}} - P_{\text{summer}}|$ ; mm) plotted with respect to latitude, showing increased precipitation seasonality at low latitude sites. We note that all sites with  $\Delta(\delta^{18}\text{O}_{\text{MW}}) < 0\text{\textperthousand}$  (Eq. (2)) were located within  $37^{\circ}$  of the equator (between the dashed lines), where seasonal changes in precipitation are the greatest.

results in a lower depletion rate than is determined when only examining low latitude sites. For example, we calculate  $A = 0.0165\text{\textperthousand}/\text{mm}$  for sites within  $30^{\circ}$  latitude of the equator, which is nearly the same as the published values for these regions determined using other methods (see above). We note that further optimization of our equations for specific regions of the world may increase the correlation coefficients and reduce the scatter between the measured and modeled values; however, this regional information may not be available when applying this work to fossil wood. Therefore, we choose to use our globally optimized rate of  $0.0082\text{\textperthousand}/\text{mm}$  in order to maintain the greatest applicability within the fossil record.

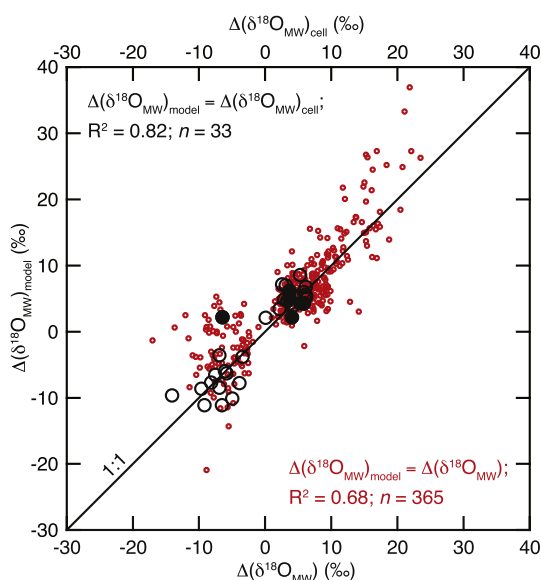


**Fig. 7.** Correlation between the measured seasonal change in the oxygen isotope value of meteoric water, as calculated from the GNIP database [ $\Delta(\delta^{18}\text{O}_{\text{MW}})$ ], versus estimates using Eq. (7) [ $\Delta(\delta^{18}\text{O}_{\text{MW}})_{\text{model}}$ ] (red points,  $n = 365$ ). Also shown is the correlation between the seasonal change in the oxygen isotope value of meteoric water as calculated from intra-ring  $\delta^{18}\text{O}_{\text{cell}}$  measurements [ $\Delta(\delta^{18}\text{O}_{\text{MW}})_{\text{cell}}$ ; Eq. (3) with  $M = 0.66$ ] versus estimates using Eq. (7) [ $\Delta(\delta^{18}\text{O}_{\text{MW}})_{\text{model}}$ ; black circles,  $n = 33$ ]. Closed circles represent the five new tree-ring sites; open circles represent the 28 published tree-ring sites.

### 3.6. Eq. (7) as a unified method for incorporating the effects of seasonal climate upon intra-annual changes in the oxygen isotope composition of meteoric water

Multiple previous workers have examined how temperature and precipitation affect the seasonal change in  $\delta^{18}\text{O}$  measured in precipitation (e.g., Araguás-Araguás et al., 1998; Bowen, 2008; Dansgaard, 1964; Rozanski et al., 1992, 1993). For example, Bowen (2008) used the GNIP database to compare the magnitude of the intra-annual  $\delta^{18}\text{O}_{\text{MW}}$  signal to slope coefficients for the regression of long-term monthly average  $\delta^{18}\text{O}_{\text{MW}}$  on temperature and precipitation made at individual sites. This work produced maps showing spatial variation in the slopes of these relationships across all land areas. Bowen (2008) noted, however, that temperature and precipitation are often autocorrelated, which makes separating these effects difficult. For this reason, we independently determined the temperature relationship first (Eqs. (4) and (6)), and only then did we proceed to optimize the precipitation coefficient ( $A$ ). Furthermore,  $\Delta(\delta^{18}\text{O}_{\text{MW}})$  values can be positive (Eq. (2A)) or negative (Eq. (2B)), which makes our analysis applicable to the many sites that show an inverse relationship between temperature and  $\delta^{18}\text{O}_{\text{MW}}$  due to a strong seasonal precipitation component (e.g., monsoon climates). Lastly, our analysis quantified the temperature effect using a hyperbolic, rather than linear relationship to better approximate the data, which shows a decrease in the effect of temperature on  $\delta^{18}\text{O}_{\text{MW}}$  as temperatures increase (Fig. 4). In this way, a  $10^{\circ}\text{C}$  seasonal change in temperature from  $-10$  to  $0^{\circ}\text{C}$ , for example, would result in a greater expected intra-annual change in  $\delta^{18}\text{O}_{\text{MW}}$  ( $5.0\text{\textperthousand}$ ) than a  $10^{\circ}\text{C}$  seasonal change in temperature from  $20$  to  $30^{\circ}\text{C}$  ( $2.7\text{\textperthousand}$ ) (Eq. (6)).

The residual between the measured and modeled  $\Delta(\delta^{18}\text{O}_{\text{MW}})$  value [residual =  $\Delta(\delta^{18}\text{O}_{\text{MW}}) - \Delta(\delta^{18}\text{O}_{\text{MW}})_{\text{model}}$ ] associated with each site was poorly correlated with site distance (in degrees latitude) from the equator ( $R^2 = 0.06$ ). We note, however, that the residual was closer to zero for sites warm enough to support forested ecosystems: i.e., at sites with  $\text{MAT} > -5^{\circ}\text{C}$  ( $n = 342$ ) or  $T_{\min} \geq -25^{\circ}\text{C}$  ( $n = 348$ ) the residual averaged only  $-0.59\text{\textperthousand}$  and  $-0.64\text{\textperthousand}$ , respectively. In contrast, residuals were highest at very cold sites: sites with  $\text{MAT} < -5^{\circ}\text{C}$  ( $n = 23$ ) or  $T_{\min} < -25^{\circ}\text{C}$  ( $n = 17$ ) averaged residuals of  $-6.5\text{\textperthousand}$  and  $-7.6\text{\textperthousand}$ , respectively. In addition, the absolute magnitude of the residual increased with decreasing  $T_{\min}$  for sites with  $T_{\min} < 0^{\circ}\text{C}$  ( $R^2 = 0.33$ ;  $P < 0.0001$ ;  $n = 118$ ). Based upon the above, we propose that seasonal changes in temperature and precipitation (the model described by Eq. (7)) can be used to accurately predict intra-annual changes in  $\delta^{18}\text{O}_{\text{MW}}$  across a wide geographic range of modern environments. We note that while error is increased within cold tundra environments, precision is highest across the Earth's environments that support a diverse array of forested ecosystems, the very environments that tend to produce wood suitable for high-resolution intra-annual isotope analysis (Schubert and Jahren, 2011).

### 3.7. Relating the intra-annual change in the oxygen isotope compositions of wood cellulose to seasonal climate

In order to evaluate the potential of using intra-ring  $\delta^{18}\text{O}_{\text{cell}}$  measurements to quantify seasonal climate, we plotted  $\Delta(\delta^{18}\text{O}_{\text{MW}})_{\text{cell}}$  values (Eq. (3)) versus the  $\Delta(\delta^{18}\text{O}_{\text{MW}})_{\text{model}}$  values calculated using Eq. (7) with  $T_{\max}$ ,  $T_{\min}$ ,  $P_{\text{winter}}$ ,  $P_{\text{summer}}$  values available for each of the 33 sites. The resultant agreement ( $R^2 = 0.82$ ) is shown in Fig. 7. For all 33 of the tree-ring sites, the average absolute difference between the cellulose-derived estimate of  $\Delta(\delta^{18}\text{O}_{\text{MW}})$  [ $\Delta(\delta^{18}\text{O}_{\text{MW}})_{\text{cell}}$ ] and the climate-based estimate [ $\Delta(\delta^{18}\text{O}_{\text{MW}})_{\text{model}}$ ] was  $2.2 \pm 2.1\text{\textperthousand}$  ( $\pm 1\sigma$ ,  $n = 33$ ), which was actually less than the average absolute difference of  $3.0 \pm 3.0\text{\textperthousand}$  ( $\pm 1\sigma$ ,  $n = 365$ ) determined between the measured

$[\Delta(\delta^{18}\text{O}_{\text{MW}})]$  and modeled  $[\Delta(\delta^{18}\text{O}_{\text{MW}})_{\text{model}}]$  values in the modern precipitation dataset ( $P = 0.06$ ). The average residual between the  $\Delta(\delta^{18}\text{O}_{\text{MW}})_{\text{cell}}$  value and the  $\Delta(\delta^{18}\text{O}_{\text{MW}})_{\text{model}}$  value was  $-0.7 \pm 2.8\%$  ( $\pm 1\sigma, n = 33$ ). Because there was a wide range in the number of tree rings sampled at each site (2–301 rings, median = 5 rings; Table 1), we examined whether the absolute magnitude of the residual decreased with an increase in the number of rings sampled, but found no such trend ( $R^2 = 0.03, P = 0.38, n = 33$ ). This suggests that the relatively low numbers of rings sampled in most studies (over half sampled only 2 to 5 rings) are sufficient for accurately reconstructing seasonal changes in  $\delta^{18}\text{O}_{\text{MW}}$  from intra-ring  $\delta^{18}\text{O}_{\text{cell}}$  measurements. For longer records, seasonal changes in  $\delta^{18}\text{O}_{\text{MW}}$  could therefore be reconstructed in sub-decadal (~2–5 year) sections.

Based on the excellent agreement between measured and modeled data shown in (Fig. 7), we put forth a method for using intra-ring isotope data to quantify the seasonal climate of both temperature and precipitation. By combining Eqs. (3) and (7), we present here an equation modeling the intra-annual change in  $\delta^{18}\text{O}_{\text{cell}}$  [ $\Delta(\delta^{18}\text{O}_{\text{cell}})_{\text{model}}$ ] with seasonal changes in temperature and precipitation:

$$\Delta(\delta^{18}\text{O}_{\text{cell}})_{\text{model}} = [(17.57T_{\text{max}})/(39.89 + 0.44T_{\text{max}}) - (17.57T_{\text{min}})/(39.89 + 0.44T_{\text{min}}) + A(P_{\text{winter}} - P_{\text{summer}})] * M \quad (8)$$

where  $T_{\text{min}} \geq 0^\circ\text{C}$ ,  $A = 0.0082$ , and  $M = 0.66$ . When we compared the value of  $\Delta(\delta^{18}\text{O}_{\text{cell}})$  that we obtained from wood samples (Eq. (1)) to the value of  $\Delta(\delta^{18}\text{O}_{\text{cell}})_{\text{model}}$  calculated for each site using Eq. (8) in conjunction with local climate data, we observed an excellent agreement ( $R^2 = 0.82$ ) (this is the same value determined between  $\Delta(\delta^{18}\text{O}_{\text{MW}})_{\text{cell}}$  and  $\Delta(\delta^{18}\text{O}_{\text{MW}})_{\text{model}}$  because Eq. (8) is simply a scaled version of Eq. (7)). The value of  $A = 0.0082$ , which was optimized for the modern GNIP  $\Delta\delta^{18}\text{O}_{\text{MW}}$  dataset, is nearly identical to the value that yields the highest correlation with the  $\Delta(\delta^{18}\text{O}_{\text{MW}})_{\text{cell}}$  dataset ( $R^2 = 0.82$  for  $A = 0.0082$ ;  $R^2 = 0.83$  for  $A = 0.0091$ ). The tree-ring dataset (Table 1) shown in Fig. 8 suggests that Eq. (8) is applicable to diverse tree species with different leaf morphologies and growth strategies growing under a wide range of climate conditions.

### 3.8. Incorporation of high-resolution carbon and oxygen isotope profiles across tree rings in order to quantify seasonal climate

Because Eq. (8) contains four unknown terms (i.e.,  $T_{\text{max}}$ ,  $T_{\text{min}}$ ,  $P_{\text{winter}}$ , and  $P_{\text{summer}}$ ), additional information is required to solve for any one of these variables using high-resolution  $\delta^{18}\text{O}_{\text{cell}}$  records. We have previously shown that the average seasonal change in the carbon isotope value [ $\Delta(\delta^{13}\text{C})$ ] measured across tree rings of a wide range of evergreen species growing in diverse environments reflects changes in the ratio of summer to winter precipitation amount ( $P_{\text{summer}}/P_{\text{winter}}$ ) ( $R^2 = 0.96$ ), after seasonal changes in the carbon isotopic composition of atmospheric carbon dioxide [ $\Delta(\delta^{13}\text{C}_{\text{CO}_2})$ ] are taken into account (Schubert and Jahren, 2011):

$$\Delta(\delta^{13}\text{C}) = \Delta(\delta^{13}\text{C}_{\text{CO}_2}) - 0.82[\ln(P_{\text{summer}}/P_{\text{winter}})] + 0.73. \quad (9)$$

Within the above,  $P_{\text{summer}}$  and  $P_{\text{winter}}$  represent the average total precipitation during the 6-month period (May through October or November through April) during which the maximum and minimum  $\delta^{13}\text{C}$  values occurred, respectively. The value of  $\Delta(\delta^{13}\text{C}_{\text{CO}_2})$  is calculated based on the latitude of the site [ $\Delta(\delta^{13}\text{C}_{\text{CO}_2}) = 0.01L + 0.13$ , for sites north of  $8^\circ\text{S}$  latitude;  $\Delta(\delta^{13}\text{C}_{\text{CO}_2}) = 0.05\%$  for sites south of  $8^\circ\text{S}$  latitude]. Because mean annual precipitation (MAP) at any site can be written as the sum of

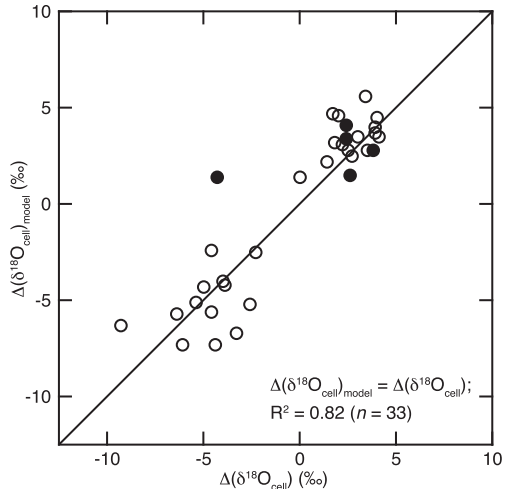


**Fig. 8.** Comparison between the  $\Delta(\delta^{18}\text{O}_{\text{cell}})$  value measured within tree rings from each of the 33 sites shown in Fig. 1 and the value of  $\Delta(\delta^{18}\text{O}_{\text{cell}})_{\text{model}}$  calculated using known climate characteristics and Eq. (8), showing excellent agreement between the measured and modeled values ( $R^2 = 0.82$ ). Closed circles represent the five new tree-ring sites; open circles represent the 28 published tree-ring sites.

average total summer and winter precipitation:

$$\text{MAP} = P_{\text{summer}} + P_{\text{winter}}, \quad (10)$$

Eqs. (9) and (10) can be solved simultaneously to quantify average total summer and winter precipitation amounts, provided that there exists an independent estimate of MAP. Estimates of MAP can be determined from other proxies including leaf-area analysis and bioclimatic analysis based upon nearest living relatives (Greenwood et al., 2010; Wilf et al., 1998) and paleosol data (Hyland et al., 2015; Retallack, 2005; Sheldon et al., 2002). We have previously shown the utility of solving these equations for paleoclimate reconstruction of seasonal precipitation by quantifying the relative dominance of summer precipitation within the Arctic forests of the Eocene epoch (Schubert et al., 2012).

Here we highlight the potential power of combining oxygen isotope intra-ring data with carbon isotope intra-ring data in order to solve for all of the variables in Eq. (8) (i.e.,  $P_{\text{winter}}$ ,  $P_{\text{summer}}$ ,  $T_{\text{max}}$ ,  $T_{\text{min}}$ ), provided that MAT and MAP are known, or have been estimated for a given site. We note that estimates of MAT are available for many terrestrial fossil sites using a myriad of proxies including isotopic equilibrium between terrestrial carbonate and environmental water (Jahren and Sternberg, 2003); membrane lipids of bacteria (e.g., Weijers et al., 2006); leaf-margin analysis and bioclimatic analysis (e.g., Greenwood et al., 2005, 2010); the Climate-Leaf Analysis Multivariate Program (Wolfe, 1994); combined ring width and  $\delta^{18}\text{O}$  measurements (Ballantyne et al., 2006); smectite geothermometry (Mix and Chamberlain, 2014); and the coexistence approach, which is based on the habitable climate zones of the nearest living relatives of the fossil taxa (e.g., Mosbrugger and Utescher, 1997; Popova et al., 2012).

Our inspection of a global dataset of monthly temperatures across all land areas except Antarctica (New et al., 2002) reveals that the following approximation of MAT:

$$\text{MAT} = (T_{\text{max}} + T_{\text{min}})/2 \quad (11)$$

shows excellent correlation with MAT values calculated using all 12 months of the year ( $R^2 > 0.99, n = 566,262$ ) (Fig. 9). Thus Eqs. (8)–(11), solved simultaneously, will allow for the calculation of  $P_{\text{winter}}$ ,  $P_{\text{summer}}$ ,  $T_{\text{max}}$  and  $T_{\text{min}}$  from high-resolution  $\delta^{13}\text{C}$  and  $\delta^{18}\text{O}_{\text{cell}}$

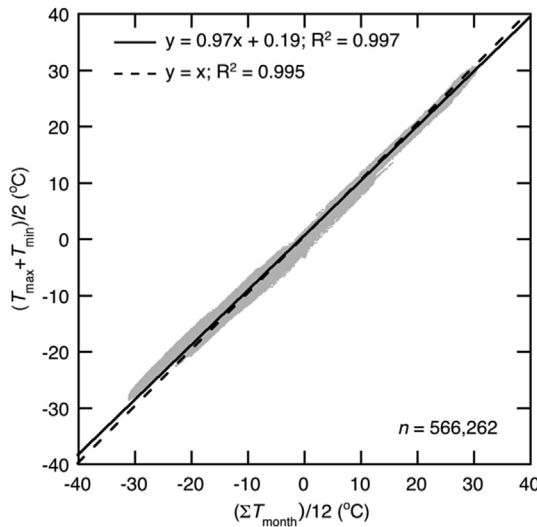


**Fig. 9.** Correlation between MAT determined by averaging monthly temperature data for all 12 months and MAT calculated as the average temperature determined only using data for the warmest ( $T_{\max}$ ) and coldest ( $T_{\min}$ ) months (Eq. (11)). Monthly temperature data used to calculate MAT were from a global dataset determined for all land areas, except Antarctica, at 10' spatial resolution (New et al., 2002).

profiles across modern or fossil wood.

We can show the validity of this technique to accurately predict seasonal climate by applying it to data from trees at modern sites with known climate conditions. Fig. 10 shows intra-ring  $\delta^{13}\text{C}$  values for three evergreen trees that we sampled for both  $\delta^{13}\text{C}$  and  $\delta^{18}\text{O}_{\text{cell}}$  data (sites 1, 4 and 5); two published studies of other sites shown in Fig. 1 (sites 21 and 28) also feature the necessary high-resolution  $\delta^{13}\text{C}$  and  $\delta^{18}\text{O}_{\text{cell}}$  data. We first determined  $P_{\text{winter}}$  and  $P_{\text{summer}}$  from the intra-ring  $\delta^{13}\text{C}$  data for the five sites using Eqs. (9) and (10) (after Schubert and Jahren, 2011; Schubert et al., 2012) and then compared these calculated values to the actual values measured at each site; the results of this comparison showed high correlation ( $R^2 = 0.98$ ) (Fig. 11A). We then used these  $\delta^{13}\text{C}$ -based estimates of  $P_{\text{winter}}$  and  $P_{\text{summer}}$  and Eqs. (8) and (11) to calculate both  $T_{\max}$  and  $T_{\min}$ . The calculated values for  $T_{\max}$  and  $T_{\min}$  also showed excellent agreement with reported temperature data for each site (Fig. 11B;  $R^2 = 0.91$ ). These results confirm that across diverse sites and tree species, seasonal climate ( $T_{\max}$ ,  $T_{\min}$ ,  $P_{\text{winter}}$ , and  $P_{\text{summer}}$ ) can be accurately quantified using a combination of carbon and oxygen intra-ring isotope profiles.

#### 4. Conclusions and implications for reconstructing paleoclimate seasonality

Our analysis shows that average intra-annual changes in  $\delta^{18}\text{O}_{\text{cell}}$  measured across tree rings (Fig. 2) do in fact reflect average seasonal changes in  $\delta^{18}\text{O}_{\text{MW}}$  (Eq. (3); Fig. 3) and these seasonal changes in  $\delta^{18}\text{O}_{\text{MW}}$  are in turn affected by the average seasonal climate (Eq. (7)). The strong correlation between the measured and modeled  $\Delta(\delta^{18}\text{O}_{\text{cell}})$  values (Fig. 8) demonstrates the potential for Eq. (8) to be used to reconstruct average seasonality using ancient tree-rings. The augmentation of  $\delta^{18}\text{O}$  data with  $\delta^{13}\text{C}$  can be used to solve for more variables, allowing for the quantification of multiple aspects of paleoclimate, including both temperature and precipitation. The work presented here is based on empirical relationships from global datasets, but may not be applicable to certain environments. For example, studies have shown that within fog-dominated ecosystems (Anchukaitis et al., 2008; Roden et al., 2009), semiarid environments (Kanner et al., 2014), or regions where seasonal

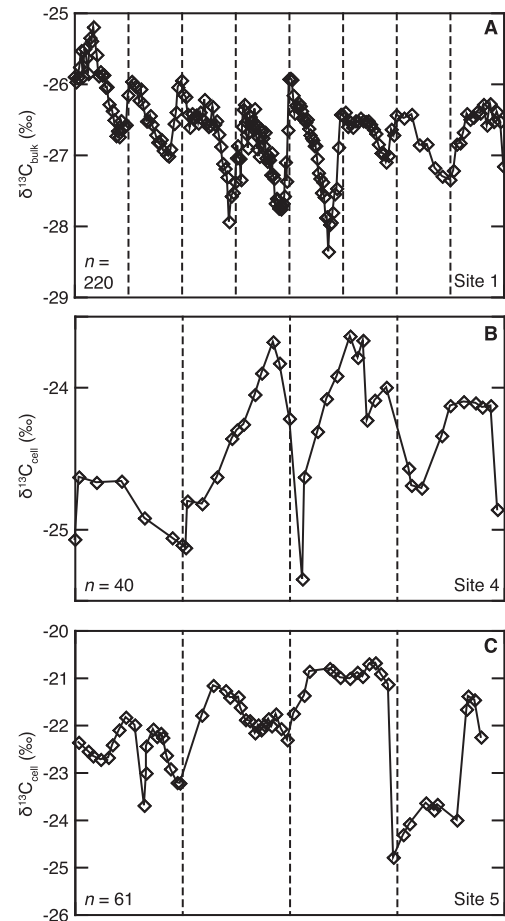


**Fig. 10.** Intra-ring carbon isotope data for the three evergreen trees also analyzed for  $\delta^{18}\text{O}_{\text{cell}}$  in this study. Dashed, vertical lines denote ring boundaries; the direction of growth is left to right. The three profiles represent (A) Mauna Kea, Hawaii (Site 1;  $\Delta(\delta^{13}\text{C}_{\text{bulk}}) = 1.30\text{‰}$ ); (B) Palmer, Alaska (Site 4;  $\Delta(\delta^{13}\text{C}_{\text{cell}}) = 1.05\text{‰}$ ); and (C) Ås, Norway (Site 5;  $\Delta(\delta^{13}\text{C}_{\text{cell}}) = 1.38\text{‰}$ ,  $\Delta(\delta^{13}\text{C})$  values were calculated as the average difference between the maximum  $\delta^{13}\text{C}$  value of a given year and the preceding minimum  $\delta^{13}\text{C}$  value of the annual cycle (after Schubert and Jahren, 2011). Data from Mauna Kea, Hawaii (A) represents bulk wood measurements from Schubert and Jahren (2011); data from Palmer, Alaska (B) and Ås, Norway (C) are new carbon isotope measurements made on the same cellulose samples extracted for  $\delta^{18}\text{O}$  analyses (Fig. 2).

variation in  $\delta^{18}\text{O}_{\text{MW}}$  is affected by large-scale vapor transport patterns (Bowen, 2008; Bowen and Wilkinson, 2002; Breecker, 2013; Liu et al., 2013; Saurer et al., 2012) the local effects of changes in moisture source on the intra-annual  $\delta^{18}\text{O}_{\text{cell}}$  pattern may be important. Our dataset does include such ecosystems [e.g., site 26 (significant fog); sites 1, 4, 11–13 (dry, MAP < 500 mm); sites 6, 16, 18–19, 22–25, 30–31 (monsoonal)] and our model using only changes in seasonal temperature and precipitation amount does successfully explain much of the variability in the measured intra-ring  $\delta^{18}\text{O}_{\text{cell}}$  signal worldwide ( $R^2 = 0.82$ ) (Fig. 8), but this relationship could be refined on a case-by-case basis for a specific locality subject to any of the phenomena itemized above. In addition, the analysis described here only investigates average conditions and does not investigate inter-annual variability in the seasonal signal.

Much work has been done to show that the quality of information gained from intra-ring isotope analysis is dependent upon several factors, including sampling frequency/resolution across the tree rings (Schubert and Jahren, 2011), inconsistent growth rates and/or tree-rooting depth (Rinne et al., 2013; Sarris et al., 2013), the impact of snowmelt on the  $\delta^{18}\text{O}$  value of tree-ring cellulose at the

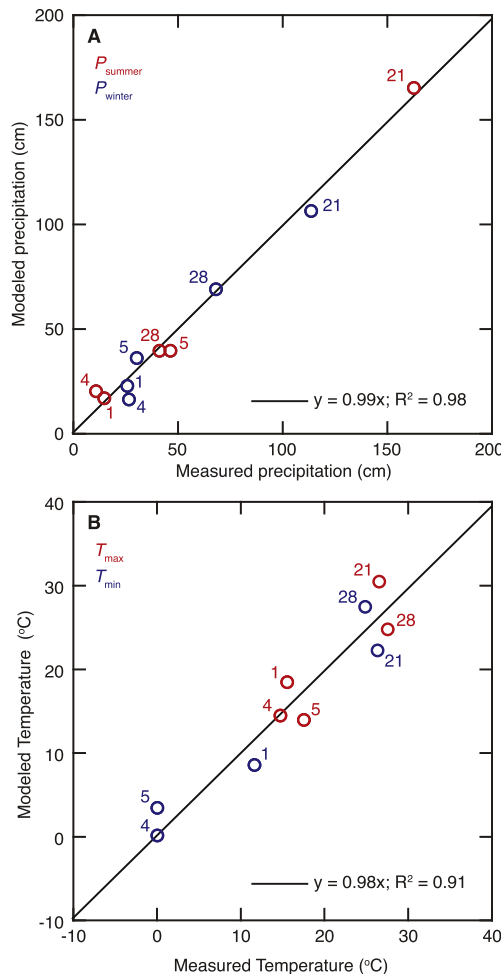


**Fig. 11.** Correlation between measured and modeled precipitation (A) and temperature (B) data for five of the sites shown on Fig. 1 that contain both high-resolution  $\delta^{13}\text{C}$  and  $\delta^{18}\text{O}_{\text{cell}}$  data from evergreen species (Sites 1, 4, 5, 21, and 28; Table 1). For each site, modeled values for  $P_{\text{summer}}$  and  $P_{\text{winter}}$  (panel A) were calculated by solving Eqs. (9) and (10) simultaneously using independent measurements of MAP (Table 2) and  $\Delta(\delta^{13}\text{C})$  values determined within Fig. 10 (Sites 1, 4, and 5) and Schubert and Jahren (2011) (Sites 21 and 28). Modeled values for  $T_{\max}$  and  $T_{\min}$  (panel B) were calculated by solving Eqs. (8) and (11) using the modeled ( $\delta^{13}\text{C}$ -based)  $P_{\text{summer}}$  and  $P_{\text{winter}}$  values shown in panel (A), and data presented within Table 2.

beginning of the growing season (Knorr et al., 2010; Vaganov et al., 1999), and decreases in the intra-annual  $\delta^{18}\text{O}$  signal of river or ground water relative to that of precipitation due to mixing (Dutton et al., 2005). Our analysis shows that the variation in  $\Delta(\delta^{18}\text{O}_{\text{cell}})$  measured across diverse sites (each presumably subject to many of the above) can be effectively approximated quantitatively using the variability in seasonal temperature and precipitation amount. Plant characteristics that are known to affect absolute  $\delta^{18}\text{O}_{\text{cell}}$  values, but do not change seasonally, would not affect the applicability of the equations presented above. Such characteristics include tree species (e.g., Wang et al., 1998), stomatal density (Larcher et al., 2015), and differences in leaf-water enrichment and transpiration among individual trees (e.g., Gessler et al., 2013). Likewise, absolute  $\delta^{18}\text{O}_{\text{MW}}$  values have been shown to vary as a function of geographic parameters such as elevation (altitude) or distance from the coast (e.g., Dotsika et al., 2010; Dutton et al., 2005; Garzione et al., 2000; Gonfiantini et al., 2001; Rozanski et al., 1993), but these too, do not change seasonally. Seasonal variations in the contribution of different carbohydrate sources to tree-ring formation might introduce additional variability in deciduous species that rely on

remobilized starches to produce leaf tissue in spring (Offermann et al., 2011). We note that storm track trajectories, evapotranspiration, moisture recycling, and transport processes (e.g., advection versus eddy diffusion) can also vary seasonally and therefore likely account for some of the scatter observed in our relationships and some of the more subtle differences among sites (Winnick et al., 2014). Additional scatter may arise from non-uniform sample resolution, and inexact agreement between the meteorological data at the climate station (or  $\delta^{18}\text{O}_{\text{MW}}$  data generated by the OIPC) and the tree-ring sites. However, the robustness and general applicability of our relationships across diverse species (Table 1) growing across a wide geographic extent (Fig. 1) is illustrated by the strong correlation between the measured and modeled values determined here (Figs. 7 and 8) and bodes well for application to recent and ancient tree-ring records (e.g., Jahren and Sternberg, 2008; Schubert et al., 2012).

Our result that temperature and precipitation are the dominant drivers of the intra-annual change in  $\delta^{18}\text{O}_{\text{cell}}$  is consistent with previous interpretations made at individual sites where workers have commonly correlated intra-annual  $\delta^{18}\text{O}_{\text{cell}}$  measurements with seasonal temperature, precipitation, and/or humidity for sites with known climate records (e.g., Barbour et al., 2002; Berkelhammer and Stott, 2009; Dodd et al., 2008; Managave et al., 2010; Pons and Helle, 2011; Schollaen et al., 2013). These site-specific relationships have been used to calibrate a local climate proxy based on intra-annual  $\delta^{18}\text{O}_{\text{cell}}$  measurements (e.g., Anchukaitis et al., 2008; Ballantyne et al., 2011; Evans and Schrag, 2004; Zhu et al., 2012), although the sensitivities of different environmental variables may change through time (Kanner et al., 2013). The work we present here, however, provides a general, widely applicable relationship that can be used on modern and fossil samples. This is a particularly important result because local calibration relationships are not possible for locations or time periods for which no instrumental or independent proxy records exist (e.g., Fricke and O'Neil, 1999). Fig. 11 shows that application of Eqs. (8)–(11) is robust across different genera representing angiosperm and gymnosperm trees growing under a wide range of climate conditions worldwide. The wide applicability of this relationship to diverse climates, species, and geographic locations makes it particularly relevant to reconstructing climate from modern and fossil tree rings. While analyzing for oxygen isotopes from extracted cellulose, it is relatively simple to include a carbon isotope measurement, allowing for the convenient production of all data necessary to use Eqs. (8)–(11) to expand on reconstructions of mean annual temperature to solve quantitatively for seasonal temperature. Such valuable insight into seasonal change in climate parameters represents an advance in our understanding of paleoclimate, over previous interpretations built only upon mean annual estimates.

## Acknowledgments

We thank W.M. Hagopian, N.E. Parker, and S.K. Salisbury for analytical assistance; P. Hart, A. Timmermann, A. Steffenrem, and H. Kvaalen for tree core samples; and S. Kulseng at Røkenes Gård (Harstad, Norway) and the Norwegian University of Life Sciences Environmental Sciences Department for access to the experimental forest in Ås, Norway. The tree core at Harstad, Norway was collected as part of the WoodWisdom-Net Research Programme project 2006–11 WOVEN. This work was supported by NSF/EAR Grant 1250063 and US FWS Grant 12170-B-G103, and a Fulbright Award to AHJ.

## Appendix A. Supplementary data

Supplementary data related to this article can be found at <http://dx.doi.org/10.1016/j.quascirev.2015.07.024>.

## References

- Anchukaitis, K.J., Evans, M.N., Wheelwright, N.T., Schrag, D.P., 2008. Stable isotope chronology and climate signal calibration in neotropical montane cloud forest trees. *J. Geophys. Res.* 113 <http://dx.doi.org/10.1029/2007jg000613>.
- Araguás-Araguás, L., Froehlich, K., Rozanski, K., 1998. Stable isotope composition of precipitation over southeast Asia. *J. Geophys. Res.* 103, 28721–28742.
- Ballantyne, A.P., Baker, P.A., Chambers, J.Q., Villalba, R., Argollo, J., 2011. Regional differences in South American monsoon precipitation inferred from the growth and isotopic composition of tropical trees. *Earth Interact.* 15, 1–35.
- Ballantyne, A.P., Rybcynski, N., Baker, P.A., Harrington, C.R., White, D., 2006. Pliocene Arctic temperature constraints from the growth rings and isotopic composition of fossil larch. *Palaeogeogr. Palaeoclimatol. Palaeoecol.* 242, 188–200.
- Barbour, M.M., Walcroft, A.S., Farquhar, G.D., 2002. Seasonal variation in  $\delta^{13}\text{C}$  and  $\delta^{18}\text{O}$  of cellulose from growth rings of *Pinus radiata*. *Plant Cell Environ.* 25, 1483–1499.
- Berkelhammer, M., Stott, L.D., 2009. Modeled and observed intra-ring  $\delta^{18}\text{O}$  cycles within late Holocene Bristlecone Pine tree samples. *Chem. Geol.* 264, 13–23.
- Bowen, G.J., 2008. Spatial analysis of the intra-annual variation of precipitation isotope ratios and its climatological corollaries. *J. Geophys. Res.* 113, D05113.
- Bowen, G.J., 2013. The Online Isotopes in Precipitation Calculator. <http://www.waterisotopes.org>, 2.2.
- Bowen, G.J., Ravenaugh, J., 2003. Interpolating the isotopic composition of modern meteoric precipitation. *Water Resour. Res.* 39, 1299. <http://dx.doi.org/10.1029/2003WR002086>.
- Bowen, G.J., Wassenaar, L.I., Hobson, K.A., 2005. Global application of stable hydrogen and oxygen isotopes to wildlife forensics. *Oecologia* 143, 337–348.
- Bowen, G.J., Wilkinson, B.H., 2002. Spatial distribution of  $\delta^{18}\text{O}$  in meteoric precipitation. *Geology* 30, 315–318.
- Brand, W.A., Coplen, T.B., Aerts-Bijma, A.T., Bohlke, J.K., Gehre, M., Geilmann, H., Groning, M., Jansen, H.G., Meijer, H.A.J., Mroczkowski, S.J., Qi, H.P., Soergel, K., Stuart-Williams, H., Weise, S.M., Werner, R.A., 2009. Comprehensive inter-laboratory calibration of reference materials for  $\delta^{18}\text{O}$  versus VSMOW using various on-line high-temperature conversion techniques. *Rapid Commun. Mass Spectrom.* 23, 999–1019.
- Breecker, D.O., 2013. Quantifying and understanding the uncertainty of atmospheric CO<sub>2</sub> concentrations determined from calcic paleosols. *Geochem. Geophys. Geosyst.* 14, 3210–3220.
- Brendel, O., Iannetta, P.P.M., Stewart, D., 2000. A rapid and simple method to isolate pure  $\alpha$ -cellulose. *Phytochem. Anal.* 11, 7–10.
- Brienen, R.J.W., Helle, G., Pons, T.L., Guyot, J.-L., Gloor, M., 2012. Oxygen isotopes in tree rings are a good proxy for Amazon precipitation and El Niño-Southern Oscillation variability. *Proc. Natl. Acad. Sci.* 109, 16957–16962.
- Craig, H., 1961. Isotopic variations in meteoric waters. *Science* 133, 1702–1703.
- Csank, A.Z., Fortier, D., Leavitt, S.W., 2013. Annually resolved temperature reconstructions from a late Pliocene–early Pleistocene polar forest on Bylot Island, Canada. *Palaeogeogr. Palaeoclimatol. Palaeoecol.* 369, 313–322.
- Dansgaard, W., 1964. Stable isotopes in precipitation. *Tellus* 16, 436–468.
- Dayem, K.E., Molnar, P., Battisti, D.S., Roe, G.H., 2010. Lessons learned from oxygen isotopes in modern precipitation applied to interpretation of speleothem isotope records of paleoclimate from eastern Asia. *Earth Planet. Sci. Lett.* 295, 219–230.
- Deniro, M.J., Epstein, S., 1979. Relationship between the oxygen isotope ratios of terrestrial plant cellulose, carbon dioxide, and water. *Science* 204, 51.
- Dodd, J.P., Patterson, W.P., Holmden, C., Brasseur, J.M., 2008. Robotic micromilling of tree-rings: a new tool for obtaining subseasonal environmental isotope records. *Chem. Geol.* 252, 21–30.
- Dotsika, E., Lykoudis, S., Poutoukis, D., 2010. Spatial distribution of the isotopic composition of precipitation and spring water in Greece. *Glob. Planet. Change* 71, 141–149.
- Dutton, A., Wilkinson, B.H., Welker, J.M., Bowen, G.J., Lohmann, K.C., 2005. Spatial distribution and seasonal variation in  $\delta^{18}\text{O}/\delta^{16}\text{O}$  of modern precipitation and river water across the conterminous USA. *Hydrol. Process.* 19, 4121–4146.
- Evans, M.N., Schrag, D.P., 2004. A stable isotope-based approach to tropical dendroclimatology. *Geochim. Cosmochim. Acta* 68, 3295–3305.
- Fricke, H.C., O'Neil, J.R., 1999. The correlation between  $\delta^{18}\text{O}/\delta^{16}\text{O}$  ratios of meteoric water and surface temperature: its use in investigating terrestrial climate change over geologic time. *Earth Planet. Sci. Lett.* 170, 181–196.
- Garzione, C.N., Quade, J., DeCelles, P.G., English, N.B., 2000. Predicting paleo-elevation of Tibet and the Himalaya from  $\delta^{18}\text{O}$  vs. altitude gradients in meteoric water across the Nepal Himalaya. *Earth Planet. Sci. Lett.* 183, 215–229.
- Gat, J.R., Matsui, E., 1991. Atmospheric water balance in the Amazon Basin: an isotopic evapotranspiration model. *J. Geophys. Res.* 96, 13179–13188.
- Gaudinski, J.B., Dawson, T.E., Quideau, S., Schuur, E.A.G., Roden, J.S., Trumbore, S.E., Sandquist, D.R., Oh, S.-W., Wasylshen, R.E., 2005. Comparative analysis of cellulose preparation techniques for use with  $^{13}\text{C}$ ,  $^{14}\text{C}$ , and  $\delta^{18}\text{O}$  isotopic measurements. *Anal. Chem.* 77, 7212–7224.
- Gessler, A., Brandes, E., Buchmann, N., Helle, G., Rennenberg, H., Barnard, R.L., 2009. Tracing carbon and oxygen isotope signals from newly assimilated sugars in the leaves to the tree-ring archive. *Plant Cell Environ.* 32, 780–795.
- Gessler, A., Brandes, E., Keitel, C., Boda, S., Kayler, Z.E., Granier, A., Barbour, M., Farquhar, G.D., Treydte, K., 2013. The oxygen isotope enrichment of leaf-exported assimilates – does it always reflect lamina leaf water enrichment? *New Phytol.* 200, 144–157.
- Gonfiantini, R., Roche, M.-A., Olivry, J.-C., Fontes, J.-C., Zuppi, G.M., 2001. The altitude effect on the isotopic composition of tropical rains. *Chem. Geol.* 181, 147–167.
- Green, J.W., 1963. Wood cellulose. *Methods Carbohydr. Chem.* III, 9–21.
- Greenwood, D.R., Archibald, S.B., Mathewes, R.W., Moss, P.T., 2005. Fossil biotas from the Okanagan Highlands, southern British Columbia and northeastern Washington State: climates and ecosystems across an Eocene landscape. *Can. J. Earth Sci.* 42, 167–185.
- Greenwood, D.R., Basinger, J.F., Smith, R.Y., 2010. How wet was the Arctic Eocene rain forest? Estimates of precipitation from Paleogene Arctic macrofloras. *Geology* 28, 15–18.
- Griffith, J.D., Willcox, S., Powers, D.W., Nelson, R., Baxter, B.K., 2008. Discovery of abundant cellulose microfibers encased in 250 Ma Permian halite: a macromolecular target in the search for life on other planets. *Astrobiology* 8, 215–228.
- Hyland, E.G., Sheldon, N.D., Van der Voo, R., Badgley, C., Abrjevitch, A., 2015. A new paleoprecipitation proxy based on soil magnetic properties: implications for expanding paleoclimate reconstructions. *Geol. Soc. Am. Bull.* <http://dx.doi.org/10.1130/B31207.1>.
- IAEA/WMO, 2006. Global Network of Isotopes in Precipitation. The GNIP Database Accessible at: <http://www.iaea.org/water>.
- Jahren, A.H., Sternberg, L.S.L., 2002. Eocene meridional weather patterns reflected in the oxygen isotopes of Arctic fossil wood. *GSA Today* 12, 4–9.
- Jahren, A.H., Sternberg, L.S.L., 2003. Humidity estimate for the middle Eocene Arctic rain forest. *Geology* 31, 463–466.
- Jahren, A.H., Sternberg, L.S.L., 2008. Annual patterns within tree rings of the Arctic middle Eocene (ca. 45 Ma): isotopic signatures of precipitation, relative humidity, and deciduousness. *Geology* 36, 99–102.
- Jouzel, J., Froehlich, K., Schotterer, U., 1997. Deuterium and oxygen-18 in present-day precipitation: data and modelling. *Hydrolog. Sci. J.* 42, 747–763.
- Kanner, L., Buenneng, N., Stott, L., Stahle, D., 2013. Climatologic and hydrologic influences on the oxygen isotope ratio of tree cellulose in coastal southern California during the late 20th century. *Geochem. Geophys. Geosyst.* 14, 4488–4503.
- Kanner, L.C., Buenneng, N.H., Stott, L.D., Timmermann, A., Noone, D., 2014. The role of soil processes in  $\delta^{18}\text{O}$  terrestrial climate proxies. *Glob. Biogeochem. Cycles* 28, <http://dx.doi.org/10.1002/2013GB004742>.
- Knorre, A.A., Siegwolf, R.T.W., Saurer, M., Sidorova, O.V., Vaganov, E.A., Kirydanov, A.V., 2010. Twentieth century trends in tree ring stable isotopes ( $\delta^{13}\text{C}$  and  $\delta^{18}\text{O}$ ) of *Larix sibirica* under dry conditions in the forest steppe in Siberia. *J. Geophys. Res. Biogeosci.* 115 <http://dx.doi.org/10.1029/2009jg000930>.
- Lachnit, M.S., Patterson, W.P., 2006. Use of correlation and stepwise regression to evaluate physical controls on the stable isotope values of Panamanian rain and surface waters. *J. Hydrol.* 324, 115–140.
- Lachnit, M.S., Patterson, W.P., 2009. Oxygen isotope values of precipitation and surface waters in northern Central America (Belize and Guatemala) are dominated by temperature and amount effects. *Earth Planet. Sci. Lett.* 284, 435–446.
- Larcher, L., Hara-Nishimura, I., Sternberg, L., 2015. Effects of stomatal density and leaf water content on the  $\delta^{18}\text{O}$  enrichment of leaf water. *New Phytol.* 206, 141–151.
- Li, Z.-H., Labbé, N., Driese, S.G., Grissino-Mayer, H.D., 2011. Micro-scale analysis of tree-ring  $\delta^{18}\text{O}$  and  $\delta^{13}\text{C}$  on  $\alpha$ -cellulose spline reveals high-resolution intra-annual climate variability and tropical cyclone activity. *Chem. Geol.* 284, 138–147.
- Liu, Z., Bowen, G., Welker, J., Yoshimura, K., 2013. Winter precipitation isotope slopes of the contiguous USA and their relationship to the Pacific/North American (PNA) pattern. *Clim. Dyn.* 41, 403–420.
- Loader, N.J., Helle, G., Los, S.O., Lehmkühl, F., Schleser, G.H., 2010. Twentieth-century summer temperature variability in the southern Altai Mountains: a carbon and oxygen isotope study of tree-rings. *Holocene* 20, 1149–1156.
- Loader, N.J., McCarroll, D., Gagen, M., Robertson, I., Jalkanen, R., 2007. Extracting climatic information from stable isotopes in tree rings. In: Dawson, T.E., Siegwolf, R.T.W. (Eds.), *Stable Isotopes as Indicators of Ecological Change*. Elsevier, pp. 27–48.
- Luo, Y., Sternberg, L.S.L., 1992. Hydrogen and oxygen isotopic fractionation during heterotrophic cellulose synthesis. *J. Exp. Bot.* 43, 47–50.
- Managave, S.R., Sheshshayee, M.S., Borgaonkar, H.P., Ramesh, R., 2010. Past break-monsoon conditions detectable by high resolution intra-annual  $\delta^{18}\text{O}$  analysis of tree rings. *Geophys. Res. Lett.* 37 <http://dx.doi.org/10.1029/2009gl041172>.
- McCarroll, D., Loader, N.J., 2004. Stable isotopes in tree rings. *Quat. Sci. Rev.* 23, 771–801.
- Mix, H.T., Chamberlain, C.P., 2014. Stable isotope records of hydrologic change and paleotemperature from smectite in Cenozoic western North America. *Geochim. Cosmochim. Acta* 141, 532–546.
- Mosbrugger, V., Utescher, T., 1997. The coexistence approach — a method for quantitative reconstructions of Tertiary terrestrial palaeoclimate data using plant fossils. *Palaeogeogr. Palaeoclimatol. Palaeoecol.* 134, 61–86.
- New, M., Lister, D., Hulme, M., Makin, I., 2002. A high-resolution data set of surface climate over global land areas. *Clim. Res.* 21, 1–25.
- Njitchoua, R., Sigha-Nkamdjou, L., Dever, L., Marlin, C., Sighomou, D., Nia, P., 1999. Variations of the stable isotopic compositions of rainfall events from the Cameroon rain forest, Central Africa. *J. Hydrol.* 223, 17–26.
- Offermann, C., Ferrio, J.P., Holst, J., Grote, R., Siegwolf, R., Kayler, Z., Gessler, A., 2011. The long way down—are carbon and oxygen isotope signals in the tree ring uncoupled from canopy physiological processes? *Tree Physiol.* 31, 1088–1102.
- Ogée, J., Barbour, M.M., Wingate, L., Bert, D., Bosc, A., Stievenard, M., Lambrot, C.,

- Pierre, M., Bariac, T., Loustau, D., Dewar, R.C., 2009. A single-substrate model to interpret intra-annual stable isotope signals in tree-ring cellulose. *Plant Cell Environ.* 32, 1071–1090.
- Pons, T.L., Helle, G., 2011. Identification of anatomically non-distinct annual rings in tropical trees using stable isotopes. *Trees-Struct. Funct.* 25, 83–93.
- Popova, S., Utescher, T., Gromyko, D., Bruch, A.A., Mosbrugger, V., 2012. Palaeoclimate evolution in Siberia and the Russian Far East from the Oligocene to Pliocene – evidence from fruit and seed floras. *Turk. J. Earth Sci.* 21, 315–334.
- Poussart, P.F., Evans, M.N., Schrag, D.P., 2004. Resolving seasonality in tropical trees: multi-decade, high-resolution oxygen and carbon isotope records from Indonesia and Thailand. *Earth Planet. Sci. Lett.* 218, 301–316.
- Poussart, P.F., Schrag, D.P., 2005. Seasonally resolved stable isotope chronologies from northern Thailand deciduous trees. *Earth Planet. Sci. Lett.* 235, 752–765.
- Retallack, G.J., 2005. Pedogenic carbonate proxies for amount and seasonality of precipitation in paleosols. *Geology* 33, 333–336.
- Reynolds-Henne, C.E., Saurer, M., Siegwolf, R.T.W., 2009. Temperature versus species-specific influences on the stable oxygen isotope ratio of tree rings. *Trees-Struct. Funct.* 23, 801–811.
- Richter, S.L., Johnson, A.H., Dranoff, M.M., LePage, B.A., Williams, C.J., 2008a. Oxygen isotope ratios in fossil wood cellulose: isotopic composition of Eocene- to Holocene-aged cellulose. *Geochim. Cosmochim. Acta* 72, 2744–2753.
- Richter, S.L., Johnson, A.H., Dranoff, M.M., Taylor, K.D., 2008b. Continental-scale patterns in modern wood cellulose  $\delta^{18}\text{O}$ : Implications for interpreting paleo-wood cellulose  $\delta^{18}\text{O}$ . *Geochim. Cosmochim. Acta* 72, 2735–2743.
- Rinne, K.T., Loader, N.J., Switsur, V.R., Waterhouse, J.S., 2013. 400-year May–August precipitation reconstruction for Southern England using oxygen isotopes in tree rings. *Quat. Sci. Rev.* 60, 13–25.
- Roden, J.S., Ehleringer, J.R., 1999. Hydrogen and oxygen isotope ratios of tree-ring cellulose for riparian trees grown long-term under hydroponically controlled environments. *Oecologia* 121, 467–477.
- Roden, J.S., Johnstone, J.A., Dawson, T.E., 2009. Intra-annual variation in the stable oxygen and carbon isotope ratios of cellulose in tree rings of coast redwood (*Sequoia sempervirens*). *Holocene* 19, 189–197.
- Rozanski, K., Araguás-Araguás, L., Gonfiantini, R., 1992. Relation between long-term trends of oxygen-18 isotope composition of precipitation and climate. *Science* 258, 981–985.
- Rozanski, K., Araguás-Araguás, L., Gonfiantini, R., 1993. Isotopic patterns in modern global precipitation. In: Swart, P.K., Lohmann, K.C., MacKenzie, J., Savin, S. (Eds.), *Climate Change in Continental Records*. American Geophysical Union, Washington, DC, pp. 1–37.
- Sarris, D., Siegwolf, R., Körner, C., 2013. Inter- and intra-annual stable carbon and oxygen isotope signals in response to drought in Mediterranean pines. *Agric. For. Meteorol.* 168, 59–68.
- Saurer, M., Borella, S., Leuenberger, M., 1997.  $\delta^{18}\text{O}$  of tree rings of beech (*Fagus sylvatica*) as a record of  $\delta^{18}\text{O}$  of the growing season precipitation. *Tellus B* 49, 80–92.
- Saurer, M., Cherubini, P., Reynolds-Henne, C.E., Treydte, K.S., Anderson, W.T., Siegwolf, R.T.W., 2008. An investigation of the common signal in tree ring stable isotope chronologies at temperate sites. *J. Geophys. Res.* 113, G04035.
- Saurer, M., Kress, A., Leuenberger, M., Rinne, K.T., Treydte, K.S., Siegwolf, R.T.W., 2012. Influence of atmospheric circulation patterns on the oxygen isotope ratio of tree rings in the Alpine region. *J. Geophys. Res. Atmos.* 117, D05118.
- Schollaen, K., Heinrich, I., Helle, G., 2014. UV-laser-based microscopic dissection of tree rings – a novel sampling tool for  $\delta^{13}\text{C}$  and  $\delta^{18}\text{O}$  studies. *New Phytol.* 201, 1045–1055.
- Schollaen, K., Heinrich, I., Neuwirth, B., Krusic, P.J., D'Arrigo, R.D., Karyanto, O., Helle, G., 2013. Multiple tree-ring chronologies (ring width,  $\delta^{13}\text{C}$  and  $\delta^{18}\text{O}$ ) reveal dry and rainy season signals of rainfall in Indonesia. *Quat. Sci. Rev.* 73, 170–181.
- Schubert, B.A., Jahren, A.H., 2011. Quantifying seasonal precipitation using high-resolution carbon isotope analyses in evergreen wood. *Geochim. Cosmochim. Acta* 75, 7291–7303 doi:10.1016/j.gca.2011.7208.7002.
- Schubert, B.A., Jahren, A.H., Eberle, J.J., Sternberg, L.S.L., Eberth, D.A., 2012. A summertime rainy season in the Arctic forests of the Eocene. *Geology* 40, 523–526.
- Sheldon, N.D., Retallack, G.J., Tanaka, S., 2002. Geochemical climofunctions from North American soils and application to paleosols across the Eocene-Oligocene boundary in Oregon. *J. Geol.* 110, 687–696.
- Sohn, J.A., Gebhardt, T., Ammer, C., Bauhus, J., Häberle, K.-H., Matyssek, R., Grams, T.E.E., 2013. Mitigation of drought by thinning: short-term and long-term effects on growth and physiological performance of Norway spruce (*Picea abies*). *For. Ecol. Manag.* 308, 188–197.
- Sternberg, L., Pinzon, M.C., Anderson, W.T., Jahren, A.H., 2006. Variation in oxygen isotope fractionation during cellulose synthesis: intramolecular and biosynthetic effects. *Plant Cell Environ.* 29, 1881–1889.
- Sternberg, L.D.L., Pinzon, M.C., Vendramini, P.F., Anderson, W.T., Jahren, A.H., Beuning, K., 2007. Oxygen isotope ratios of cellulose-derived phenyl-glucosazone: an improved paleoclimate indicator of environmental water and relative humidity. *Geochim. Cosmochim. Acta* 71, 2463–2473.
- Sternberg, L.S.L., 1989. Oxygen and hydrogen isotope measurements in plant cellulose analysis. In: Linskens, H.F., Jackson, J.F. (Eds.), *Modern Methods of Plant Analysis*. Springer-Verlag, Heidelberg, pp. 89–99.
- Sternberg, L.S.L., DeNiro, M.J., Savidge, R.A., 1986. Oxygen isotope exchange between metabolites and water during biochemical reactions leading to cellulose synthesis. *Plant Physiol.* 82, 423–427.
- Treydte, K., Boda, S., Graf Pannatier, E., Fonti, P., Frank, D., Ullrich, B., Saurer, M., Siegwolf, R., Battipaglia, G., Werner, W., Gessler, A., 2014. Seasonal transfer of oxygen isotopes from precipitation and soil to the tree ring: source water versus needle water enrichment. *New Phytol.* 202, 772–783.
- Treydte, K.S., Schleser, G.H., Helle, G., Frank, D.C., Winiger, M., Haug, G.H., Esper, J., 2006. The twentieth century was the wettest period in northern Pakistan over the past millennium. *Nature* 440, 1179–1182.
- Vaganov, E.A., Hughes, M.K., Kirdyanov, A.V., Schweingruber, F.H., Silkin, P.P., 1999. Influence of snowfall and melt timing on tree growth in subarctic Eurasia. *Nature* 400, 149–151.
- Verheyden, A., Helle, G., Schleser, G.H., Dehairs, F., Beeckman, H., Koedam, N., 2004. Annual cyclicity in high-resolution stable carbon and oxygen isotope ratios in the wood of the mangrove tree *Rhizophora mucronata*. *Plant Cell Environ.* 27, 1525–1536.
- Wang, X.-F., Yakir, D., Avishai, M., 1998. Non-climatic variations in the oxygen isotope compositions of plants. *Glob. Change Biol.* 4, 835–849.
- Waterhouse, J.S., Switsur, V.R., Barker, A.C., Carter, A.H.C., Robertson, I., 2002. Oxygen and hydrogen isotope ratios in tree rings: how well do models predict observed values? *Earth Planet. Sci. Lett.* 201, 421–430.
- Weijers, J.W.H., Schouten, S., Hopmans, E.C., Geenevasen, J.A.J., David, O.R.P., Coleman, J.M., Pancost, R.D., Sinninghe Damste, J.S., 2006. Membrane lipids of mesophilic anaerobic bacteria thriving in peats have typical archaeal traits. *Environ. Microbiol.* 8, 648–657.
- Wilf, P., Wing, S.L., Greenwood, D.R., Greenwood, C.L., 1998. Using fossil leaves as paleoprecipitation indicators: an Eocene example. *Geology* 26, 203–206.
- Wilson, A.T., Grinsted, M.J., 1978. The possibilities of deriving past climate information from stable isotope studies on tree rings. In: Robinson, B.W. (Ed.), *Stable Isotopes in the Earth Sciences*. Science Information Division, DSIR, New Zealand, pp. 61–66.
- Winnick, M.J., Chamberlain, C.P., Caves, J.K., Welker, J.M., 2014. Quantifying the isotopic ‘continental effect’. *Earth Planet. Sci. Lett.* 406, 123–133.
- Wolfe, A.P., Csank, A.Z., Reyes, A.V., McKellar, R.C., Tappert, R., Muehlenbachs, K., 2012. Pristine Early Eocene wood buried deeply in kimberlite from northern Canada. *PLoS ONE* 7, e45537.
- Wolfe, J.A., 1994. Alaskan Palaeogene climates as inferred from the CLAMP database. In: Boulter, M.C., Fisher, H.C. (Eds.), *Cenozoic Plants and Climates of the High Arctic*. Springer-Verlag, Berlin, pp. 223–238.
- Xie, L.H., Wei, G.J., Deng, W.F., Zhao, X.L., 2011. Daily  $\delta^{18}\text{O}$  and  $\delta\text{D}$  of precipitations from 2007 to 2009 in Guangzhou, South China: Implications for changes of moisture sources. *J. Hydrol.* 400, 477–489.
- Yakir, D., DeNiro, M.J., 1990. Oxygen and hydrogen isotope fractionation during cellulose metabolism in *Lemna gibba* L. *Plant Physiol.* 93, 325–332.
- Young, G.F., Loader, N., McCarroll, D., Bale, R., Demmler, J., Miles, D., Nayling, N., Rinne, K., Robertson, I., Watts, C., Whitney, M., 2015. Oxygen stable isotope ratios from British oak tree-rings provide a strong and consistent record of past changes in summer rainfall. *Clim. Dyn.* 1–14.
- Zhu, M.F., Stott, L., Buckley, B., Yoshimura, K., Ra, K., 2012. Indo-Pacific Warm Pool convection and ENSO since 1867 derived from Cambodian pine tree cellulose oxygen isotopes. *J. Geophys. Res. Atmos.* 117.